ELSEVIER

Coordination Chemistry Reviews 143 (1995)
219–263

COORDINATION CHEMISTRY REVIEWS

Phosphine-stabilized, platinum–gold and palladium–gold cluster compounds and applications in catalysis

Louis H. Pignolet *, Mark A. Aubart, Kathryn L. Craighead, Rachael A.T. Gould, Don A. Krogstad, Jack S. Wiley

The Department of Chemistry, University of Minnesota, Minneapolis, MN 55455, USA

Received 16 June 1994; revised 17 November 1994

Contents

* Corresponding author.

SSDI 0010-8545(94)07009-1

Abstract

This is a comprehensive review on the chemistry and spectroscopic properties of phosphine-stabilized, M-centered Au cluster compounds where M = platinum or palladium. The nuclearity of the clusters ranges from 3 (e.g. $[Pt(NO_3)(PPh_3)_2(AuPPh_3)_2]^+$) to 25 (e.g. $Pt_2Ag_{13}(AuPPh_3)_{10}Cl_7$). The latter consists of two Pt-centered icosahedral units sharing a common vertex. Many of the clusters contain additional metals such as Ag, Cu, or Hg in their periphery. Preparative methods are reviewed and organized by reaction type. Emphasis has been placed on reactions and transformations of preformed clusters so that the reader will acquire a useful knowledge of the reaction chemistry. Structural properties of the clusters are also described. The reactivity and structural properties of the clusters are rationalized in terms of an electron counting model and this is used throughout the review. Spectroscopic properties (e.g. nuclear magnetic resonance (NMR), fast atom bombardment mass, UV–visible, and X-ray photoelectron spectroscopy) of the clusters are described primarily for characterization; however, general trends are pointed out. Several applications in catalysis are also reviewed. Many of the clusters are good catalysts for H_2 activation and can serve as potential models for bimetallic surfaces. Kinetic data for the H_2–D_2 equilibration reaction ($H_2 + D_2 \rightleftharpoons 2HD$) are given and discussed in terms of cluster composition and structure. The results provide some insight into the well-known synergism observed for Pt—Au and Pd—Au heterogeneous catalysts. The mechanism of catalytic H_2—D_2 equilibration under homogeneous conditions is also discussed. The cluster $[Pt(AuPPh_3)_8]^{2+}$ is an excellent catalyst for $D_2(g)$–$H_2O(l)$ isotope exchange in pyridine solution. This interesting and important reaction is described and kinetic results are related to other isotope exchange systems. A tentative mechanism is proposed based on NMR analysis of the reaction mixture. Finally, prospects for future studies are given. The recent discovery of the catalytic applications of these clusters provides renewed interest in this challenging field.

Keywords: Platinum; Palladium; Phosphines; Catalysis; Clusters

1. Introduction

The area of heteronuclear gold cluster chemistry has grown enormously over the past decade and recently discovered catalytic activity with clusters of this type has revealed new directions. This review will focus on phosphine-stabilized, high nuclearity, M—Au cluster compounds (M = Pd or Pt) that contain Au—M and Au—Au bonds and a high proportion of gold in their metal framework. Clusters with these metal combinations have demonstrated a rich chemistry because of their ability to react with a wide variety of substrates. Recently it has been shown that these species also activate dihydrogen [1–3]. This review will not include homonuclear gold clusters, heteronuclear gold clusters of other metals, or M—Au clusters that are stabilized by carbon monoxide ligands. These areas have been recently reviewed by Braunstein and Rose [4], Mingos and co-workers [5,6], Pignolet and co-workers [7], Salter [8], and Steggerda [9]. Although this review will include the synthetic, reactivity, spectroscopic, and structural properties of Pt—Au and Pd—Au cluster compounds, it will emphasize reactions with H_2 and catalytic applications. There have been numerous proposals about the analogy between metal clusters and metal surfaces (see for example Ref. [10]). Although this analogy has been useful in describing the bonding modes of ligands and substrates to metal surfaces, it has been less successful in providing examples of catalytically active, intact, molecular clusters. This is especially true with bimetallic systems. It is known that the addition of gold to heterogeneous Pt and Pd catalysts has significant effects on activity and selectivity (see for example Ref. [11]). In this review we will demonstrate the great utility of these heteronuclear gold clusters in studying this synergetic effect and provide prospects for future work.

2. Comments on electron counting

Gold forms many cluster compounds with Pt and Pd (denoted M throughout this review). Several representative examples are $[M(PPh_3)(AuPPh_3)_6]^{2+}$, $[M(AuPPh_3)_8]^{2+}$, and $[M(CO)(AuPPh_3)_8]^{2+}$. These cluster compounds are air and moisture stable and soluble in common solvents such as acetone, acetonitrile, dichloromethane, and alcohols. The bonding in these high nuclearity, M-centered clusters has been described by Mingos and co-workers using a delocalized molecular orbital model derived from Stone's tensor surface harmonic theory [5,6,9,12]. An electron counting formalism has resulted from this theory and is useful in predicting structure and rationalizing reactivity [6,7,9,12–14]. The clusters can be classified as having 16 or 18 valence electrons. In the above three examples, the first two are 16-electron clusters and the third is an 18-electron cluster. As an example of electron counting for $[M(PPh_3)(AuPPh_3)_6]^{2+}$, M donates 10 electrons, PPh_3 donates 2, each $AuPPh_3$ donates 1 (6 in all), and the 2+ charge takes two away. The number of valence electrons is therefore $10+2+6-2=16$.

All the known 18-electron, heteronuclear and homonuclear gold clusters have structures in which the peripheral gold atoms and other central metal bound ligands

(such as PPh_3 and CO) lie approximately on a sphere with a spheroidal geometry, and 16-electron clusters have flattened or toroidal structures. In general, a 16-electron cluster is reactive and readily adds one 2-electron donor ligand such as CO to form an 18-electron cluster with a change in geometry from toroidal to spheroidal. An example is the reaction of $[M(AuPPh_3)_8]^{2+}$ with CO to give $[M(CO)(AuPPh_3)_8]^{2+}$. This reaction with structural representations is illustrated in Fig. 1 [15,16]. There are some exceptions to this prediction of reactivity, however. For example, $[Pt(PPh_3)(AuPPh_3)_6]^{2+}$ readily adds CO while its Pd analog does not [16,17]. This electron counting formalism provides a useful way of classifying the reactions and structures of these clusters, and will be used extensively throughout this review.

3. Preparative methods and reactivity

3.1. Preparation by direct combination of non-cluster compounds

The most straightforward method to prepare Pt—Au and Pd—Au clusters is by direct combination of monometallic Pt or Pd compounds with non-cluster Au(I) compounds such as $Au(PPh_3)X$, $X = NO_3$ or Cl, or $[(AuPPh_3)_3O]^+$. These reactions are carried out in solution with use of solvents such as acetone, methanol, or dichloromethane. Some of these reactions are illustrated in the following equations [13,18,19]:

$$Pt(PPh_3)_2(C_2H_4) + Au(PPh_3)NO_3 \rightarrow [Pt(NO_3)(PPh_3)_2(AuPPh_3)_2]^+ \quad (1)$$

$$Pt(PEt_3)_4 + Au(PPh_3)Cl \rightarrow [Pt(Cl)(PEt_3)_2(AuPPh_3)_2]^+ \quad (2)$$

$$Pt(PPh_3)_2C_2H_4 + [(AuPPh_3)_3O]^+ \xrightarrow[[NBu_4]I]{Au(PPh_3)NO_3} [Pt(I)(PPh_3)(AuPPh_3)_4]^+ \quad (3)$$

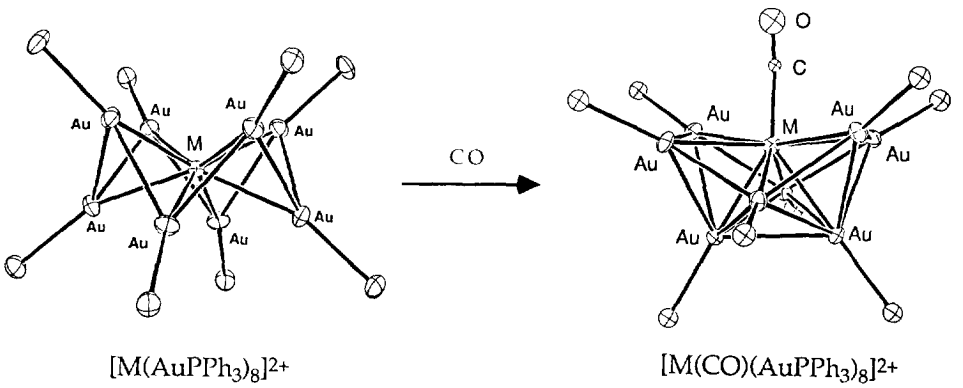

$[M(AuPPh_3)_8]^{2+}$ $[M(CO)(AuPPh_3)_8]^{2+}$

Fig. 1. Structures of the 16-electron cluster $[M(AuPPh_3)_8]^{2+}$ and the 18-electron cluster $[M(CO)(AuPPh_3)_8]^{2+}$ (M = Pd or Pt) illustrating the change in geometry from toroidal to spheroidal on the addition of CO.

Clusters of higher nuclearity are formed when this type of reaction is carried out in the presence of a reducing agent such as H_2 or $NaBH_4$ [16,20,21]:

$$Pd(acetate)_2 + Au(PPh_3)NO_3 \xrightarrow{H_2} [Pd(PPh_3)(AuPPh_3)_6]^{2+} \quad (4)$$

$$Pd(PPh_3)_4 + Au(PPh_3)NO_3 \xrightarrow{NaBH_4} [Pd(AuPh_3)_8]^{2+} \quad (5)$$

$$Pt(PPh_3)_3 + Au(PPh_3)NO_3 \xrightarrow{H_2} [Pt(H)(PPh_3)(AuPPh_3)_7]^{2+} \quad (6)$$

The $PtAu_2$ cluster formed in Eq. (1) reacts with H_2 to give the higher nuclearity $PtAu_6$ cluster $[Pt(PPh_3)(AuPPh_3)_6]^{2+}$ [17,18]:

$$[Pt(NO_3)(PPh_3)_2(AuPPh_3)_2]^{+} \xrightarrow{H_2} [Pt(PPh_3)(AuPPh_3)_6]^{2+} \quad (7)$$

The $PtAu_7$ hydrido cluster formed in Eq. (6) can be quantitatively converted into $[Pt(AuPPh_3)_8]^{2+}$ by replacement of H^+ with $[AuPPh_3]^+$ in the presence of a base [21]:

$$[Pt(H)(PPh_3)(AuPPh_3)_7]^{2+} + NEt_3 + Au(PPh_3)NO_3 \rightarrow [Pt(AuPPh_3)_8]^{2+} \quad (8)$$

The clusters illustrated in Eqs. (1)–(8) are all prepared in good yield (above 70%). The products in Eqs. (3)–(8) are the parent clusters from which most other clusters can be made (see below).

The equations which show cluster growth by reaction with reducing agents (Eqs. (4)–(7)) illustrate a general and important method of synthesizing heteronuclear and homonuclear gold clusters. For example, reduction of $Au(PPh_3)NO_3$ with $NaBH_4$ in alcohol solution gives the well-known Au_9 cluster [22]:

$$Au(PPh_3)NO_3 \xrightarrow{NaBH_4} [Au(AuPPh_3)_8]^{3+} \quad (9)$$

Reduction with use of H_2 is especially interesting and relevant in catalytic H_2 activation. The mechanism of cluster growth by H_2 reduction probably involves the oxidative addition of H_2 followed by substitution of H^+ by $AuPPh_3^+$ cations. This latter step illustrates the isolobal analogy between H^+ and $AuPPh_3^+$ [6,23,24]. Direct evidence for the H_2 oxidative addition step is provided by the reversible addition of H_2 at ambient temperature and pressure to the 16-electron cluster compound $[Pt(AuPPh_3)_8]^{2+}$ forming the 18-electron dihydride [2,3]:

$$[Pt(AuPPh_3)_8]^{2+} + H_2 \rightleftharpoons [Pt(H)_2(AuPPh_3)_8]^{2+} \quad (10)$$

This dihydride cluster has proved useful as a precursor in the synthesis of a variety of trimetallic clusters by electrophilic addition and substitution of Ag(I) and Cu(I) units (see below).

Clusters of different nuclearities can be prepared by changing the steric require-

ments of the tertiary phosphine ligands. For example, the smaller cone angle PEt_3 ligand gives the higher nuclearity $PtAu_9$ and $PtAu_{10}$ clusters compared with the $PtAu_8$ cluster formed with triaryl phosphines, PAr_3, such as PPh_3 or $P(p\text{-}CH_3C_6H_4)_3$ [3,25]:

$$Pt(PEt_3)_3 + Au(PEt_3)NO_3 \xrightarrow{H_2} [Pt(AuPEt_3)_9]^{3+} + [Pt(AuPEt_3)_{10}]^{2+} \quad (11)$$

$$Pt(PAr_3)_3 + Au(PAr_3)NO_3 \xrightarrow{H_2} [Pt(AuPAr_3)_8]^{2+} \quad (12)$$

A similar result was obtained with Au-centered clusters where the smaller cone angle PMe_2Ph ligand gave a higher nuclearity cluster than with PPh_3 [5]:

$$Au(PMe_2Ph)Cl \xrightarrow{Ti(\eta^6\text{-toluene})_2} [Au(AuPMe_2Ph)_{10}]^{3+} \quad (13)$$

$$Au(PPh_3)Cl \xrightarrow{Ti(\eta^6\text{-toluene})_2} [Au(AuPPh_3)_8]^{3+} \quad (14)$$

The introduction of even smaller ligands on some of the Au atoms, for example halides, leads to larger clusters (see below). It is expected that wider variation in phosphine ligands will lead to the synthesis of new clusters of different nuclearity and reactivity. This will provide a series of "tuned" clusters for reactivity and catalytic studies.

3.2. *Preparation by reactions of preformed clusters*

The parent cluster compounds described above undergo a number of reactions and transformations in the solution phase which lead to the preparation of new clusters. These can broadly be classified as substitution, addition, elimination, and redox reactions. A representative sampling of these and several other reactions is given below.

3.2.1. *Nucleophilic substitution of ligands*

3.2.1.1. Substitution at Au. Simple substitution of only the Au-bound ligands is uncommon as it is usually accompanied by addition or substitution at the central metal or by cluster transformation (see below). Two examples with 18-electron clusters are as follows [15,26]:

$$[Pt(CO)(AuPPh_3)_8]^{2+} + X^- \rightarrow [Pt(CO)(AuPPh_3)_7(AuX)]^+ + PPh_3 \quad (15)$$

$$(X = OR, Cl, Br, I)$$

$$[Pt(CO)(AuPPh_3)_8]^{2-} + \text{i-PrNC} \rightarrow [Pt(CO)(AuPPh_3)_7(Au\text{-i-PrNC})]^{2+} + PPh_3 \quad (16)$$

Substitution of Au-bound PPh_3 by $P(p\text{-}ClC_6H_4)_3$ or $P(p\text{-}CH_3C_6H_4)_3$ has been

observed for 16-electron clusters such as $[Pt(AuPPh_3)_8]^{2+}$ at room temperature, but the substitution is very slow and becomes detectable by ^{31}P nuclear magnetic resonance (NMR) only after several hours [3,9].

3.2.1.2. Substitution at the central metal. Simple substitution at only the central metal is also uncommon, and one example is as follows [27]:

$$[Pt(H)(PPh_3)(AuPPh_3)_7]^{2+} + SnCl_3^- \rightarrow [Pt(H)(SnCl_3)(AuPPh_3)_7]^+ + PPh_3 \quad (17)$$

3.2.2. Nucleophilic addition to 16-electron clusters

There are many examples of nucleophilic addition to the central metal of 16-electron clusters. The initial 18-electron products of these reactions often undergo further transformation leading to a large number of new cluster compounds.

3.2.2.1. Simple addition of ligands to form 18-electron clusters. Examples include the simple addition of Lewis base ligands such as CO, X^-, RNC, and $C{\equiv}C{-}C_6H_5^-$. Several are shown in the following [13,15–17]:

$$[Pt(PPh_3)(AuPPh_3)_6]^{2+} + CO \rightarrow [Pt(CO)(PPh_3)(AuPPh_3)_6]^{2+} \quad (18)$$

$$[Pt(PPh_3)(AuPPh_3)_6]^{2+} + X^- \rightarrow [Pt(X)(PPh_3)(AuPPh_3)_6]^+ \quad (19)$$

$$(X = I, Br, CN, \text{ or } C{\equiv}C{-}C_6H_5)$$

$$[M(AuPPh_3)_8]^{2+} + CO \rightarrow [M(CO)(AuPPh_3)_8]^{2+} \quad (20)$$

$$(M = Pt \text{ or } Pd)$$

The reaction of CO with $[Pd(PPh_3)(AuPPh_3)_6]^{2+}$ does not occur and with $[Pd(AuPPh_3)_8]^{2+}$ (Eq. (20)) the reaction is rapidly reversible. In Eq. (20) the Pt analog irreversibly adds CO, but with $[Pt(PPh_3)(AuPPh_3)_6]^{2+}$ (Eq. (18)) the reaction is slowly reversible.

3.2.2.2. Addition of ligands combined with substitution. Nucleophilic addition to 16-electron clusters sometimes involves substitution of ligands bound to Au and/or to the central metal, for example [15,16]:

$$[Pd(AuPPh_3)_8]^{2+} + 3P(OMe)_3 \rightarrow [Pd(P(OMe)_3(AuPPh_3)_6(AuP(OMe)_3)_2]^{2+} + 2PPh_3 \quad (21)$$

$$[Pd(PPh_3)(AuPPh_3)_6]^{2+} + 2P' \rightarrow [Pd(P^*)_2(AuPPh_3)_6]^{2+} + PPh_3 \quad (22)$$

$$(P' = P(OCH_2)_3CCH_3)$$

$$[Pt(AuPPh_3)_8]^{2+} + 2RNC \rightarrow [Pt(RNC)(AuPPh_3)_7(AuRNC)]^{2+} + PPh_3 \quad (23)$$

$$(R = i-Pr, t\text{-}Bu)$$

In all of these cases the products are 18-electron clusters. The stability and extent of substitution are dictated by a balance of steric and electronic factors.

3.2.2.3. Addition of Hg(0) to form 18-electron clusters. The addition of metallic mercury to 16-electron clusters has recently been reported [28]. A neutral Hg atom has two valence electrons so the addition of one Hg atom gives an 18-electron product [28]:

$$[Pt(PPh_3)(AuPPh_3)_6]^{2+} + Hg \rightarrow [Pt(PPh_3)(Hg)(AuPPh_3)_6]^{2+} \quad (24)$$

The Hg atom can be removed by reaction with CO [28]:

$$[Pt(PPh_3)(Hg)(AuPPh_3)_6]^{2+} + CO \rightarrow [Pt(CO)(PPh_3)(AuPPh_3)_6]^{2+} + Hg \quad (25)$$

Metallic Hg readily reacts with other 16-electron Pd—Au and Pt—Au clusters to give many new products not yet completely characterized [29].

3.2.2.4. Addition of X^- followed by fragmentation and growth. In many cases the addition of halide anions to 16-electron clusters results in cluster fragmentation and growth. Representative examples are shown in the following [26,30]:

$$[Pt(AuPPh_3)_8]^{2+} + xsX^- \rightarrow [Pt(PPh_3)(AuPPh_3)_6(AuX)_3] \quad (26)$$

$$(X = Cl, I)$$

$$[Pd(AuPPh_3)_8]^{2+} + xsBr^- \rightarrow [Pd(AuPPh_3)_7(AuBr)_3]^{+} \quad (27)$$

$$[Pd(AuPPh_3)_8]^{2+} + xsX^- \rightarrow [Pd(AuPPh_3)_8(AuX)_3] \quad (28)$$

$$(X = Cl, CN)$$

$$[Pd(AuPPh_3)_8]^{2+} + xsI^- \rightarrow [Pd(I)(AuPPh_3)_7(AuI)_2] \quad (29)$$

These reactions occur at room temperature and illustrate how the addition of a ligand to the central metal can activate the cluster. In the reaction of $[Pd(AuPPh_3)_8]^{2+}$ with I^- (Eq. (29)), the product is a rare example of a halide bound to the central metal. The products depend on the central metal, ligands, and reaction conditions. These reactions also provide good examples of how higher nuclearity clusters form when smaller ligands are available.

3.2.2.5. Addition of OCH_3^- to form cluster hydrides. One of the methods to prepare monohydride Pt—Au clusters is by nucleophilic attack of OCH_3^- on the Pt, followed by a β-H shift, and elimination of formaldehyde, OCH_2. This unusual reaction is illustrated here [27]:

$$[Pt(AuPPh_3)_8]^{2+} + OCH_3^- \rightarrow [Pt(H)(AuPPh_3)_8]^{+} + OCH_2 \quad (30)$$

$$[Pt(PPh_3)(AuPPh_3)_6]^{2+} + OCH_3^- \rightarrow [Pt(H)(PPh_3)(AuPPh_3)_6]^{+} + OCH_2 \quad (31)$$

$$[Pt(Ag)(AuPPh_3)_8]^{3+} + OCH_3^- \rightarrow [Pt(H)(Ag)(AuPPh_3)_8]^{2+} + OCH_2 \quad (32)$$

Although this is a general synthetic method for the preparation of Pt—Au cluster hydrides, it does not work with Pd—Au clusters. Indeed, there are no examples of stable Pd—Au cluster hydrides, although they have been implicated as unstable intermediates in catalysis reactions (see below) [3]. The Pt—Au cluster hydrides are stable in air but react with dilute acids to yield H_2 and the parent compounds quantitatively [27].

3.2.3. Elimination of AuL_2 on addition of PPh_3, cluster shrinking

Clusters which are sterically crowded can eliminate AuL_2 fragments to relieve their steric strain. This reaction can occur with 16- and 18-electron clusters and is stimulated by addition of PPh_3 as illustrated in the following [13]:

$$[Pt(CO)(PPh_3)(AuPPh_3)_6]^{2+} + PPh_3 \rightarrow [Pt(CO)(PPh_3)(AuPPh_3)_5]^+ + [Au(PPh_3)_2]^+ \quad (33)$$

$$[Pt(I)(PPh_3)(AuPPh_3)_4]^+ + PPh_3 \rightarrow [Pt(PPh_3)_2(AuPPh_3)_3]^+ + Au(PPh_3)I \quad (34)$$

3.2.4. Oxidative addition to 16-electron clusters

Certain substrates add to 16-electron clusters with an increase by 2 in the coordination number and the formal oxidation state of the central metal. These have been classified as oxidative addition reactions by analogy to similar reactions in organometallic chemistry. The electron count increases to 18. Several examples are illustrated in Eqs. (10), (35), and (36) [29,31,32]:

$$[Pt(AuPPh_3)_8]^{2+} + Au(CN)_2^- \rightarrow [Pt(CN)(AuCN)(AuPPh_3)_8]^+ \quad (35)$$

$$[M(AuPPh_3)_8]^{2+} + [Hg_2]^{2-} \rightarrow [M(Hg)_2(AuPPh_3)_8]^{4+} \quad (36)$$

$$(M = Pd \text{ or } Pt)$$

The addition of mercurous ion, $[Hg_2]^{2+}$, as illustrated in Eq. (36) is another method for preparing M—Au—Hg clusters.

3.2.5. Electrophilic addition of metal cations Au^+, Ag^+, or Cu^+

The addition of an electrophile does not increase the electron count of the cluster so electrophilic addition reactions occur with both 16- and 18-electron clusters. These reactions provide excellent methods of preparing tri- and tetrametallic clusters. Examples of electrophilic addition reactions to 16- and 18-electron clusters are shown in Eqs. (37) and (38) respectively [14,33]:

$$[Pt(AuPPh_3)_8]^{2+} + MX \rightarrow [Pt(MX)(AuPPh_3)_8]^{2+} \quad (37)$$

$$(MX = AgNO_3 \text{ or } CuCl)$$

$$[Pt(CO)(AuPPh_3)_8]^{2+} + MX \rightarrow [Pt(CO)(MX)(AuPPh_3)_8]^{2+} \quad (38)$$

$$(MX = AgNO_3 \text{ or } CuCl)$$

In solution the NO_3^- ligands dissociate giving clusters with bare metal atoms. Additional examples of electrophilic additions to 18-electron clusters are shown in Eqs. (39) and (40) [27,34]. An interesting example of an electrophilic substitution of isolobal ions, Ag^+ for H^+, is shown in Eq. (41) [34].

$$[Pt(H)(PPh_3)(AuPPh_3)_6]^+ + [Au(PPh_3)]^+ \rightarrow [Pt(H)(PPh_3)(AuPPh_3)_7]^{2+} \quad (39)$$

$$[Pt(H)(AgNO_3)(AuPPh_3)_8]^+ + AgNO_3 \rightarrow [Pt(H)(AgNO_3)_2(AuPPh_3)_8]^+ \quad (40)$$

$$[Pt(H)_2(AuPPh_3)_8]^{2+} + Ag^+ \rightarrow [Pt(H)(Ag)(AuPPh_3)_8]^{2+} + H^+ \quad (41)$$

Synthetic procedures can be combined to give tetrametallic clusters. Thus the addition of metallic mercury to the 16-electron product of reaction (37) gives new Pt—Au—M—Hg clusters where M = Ag or Cu [29]:

$$[Pt(MX)(AuPPh_3)_8]^{2+} + Hg \rightarrow [Pt(MX)(Hg)(AuPPh_3)_8]^{2+} \quad (42)$$

These new tetrametallic clusters have been characterized by ^{31}P NMR, fast atom bombardment mass spectroscopy (FABMS), and IR spectroscopy and for M = Ag by single-crystal X-ray diffraction [29].

3.3. Redox reactions, electrochemical transformations

The 16-electron clusters $[M(AuPPh_3)_8]^{n+}$ where M = Au ($n=3$), Pt or Pd ($n=2$) each show two reversible one-electron transfers in CH_2Cl_2 or CH_3CN solution, consistent with an EE reduction mechanism as shown in the following for $[Pd(AuPPh_3)_8]^{2+}$ [16]:

$$[Pd(AuPPh_3)_8]^{2+} + e^- \rightleftharpoons [Pd(AuPPh_3)_8]^+ + e^- \rightleftharpoons [Pd(AuPPh_3)_8] \quad (43)$$

The dependence of the potentials on M ($E_{1/2}(Au) > E_{1/2}(Pt) > E_{1/2}(Pd)$) is in the same order as found for the reduction potentials of mononuclear Au, Pt, and Pd compounds [16,35]. The difference in $E_{1/2}$ values of the two consecutive steps was greater than 100 mV, but, since comproportionation reactions are fast, 17-electron species could not be isolated as pure compounds [35]. Oxidation of 16-electron clusters led to irreversible fragmentation, and thus clusters with less than 16 electrons have not been prepared. Stable 18-electron clusters do not show reversible electrochemistry, and thus clusters with greater than 18 electrons have not been prepared [16,35].

3.4. Cluster of clusters or supracluster formation

Teo and co-workers have prepared and structurally characterized a series of Au—Ag supraclusters that contain 25, 38, and 46 metal atoms [36–38]. These supraclusters are prepared by the reduction of a mixture of Au(I) and Ag(I) species in the presence of phosphine and halide ligands. They are derived from vertex-shared, Au-centered Au_7Ag_6 icosahedral units in which the phosphine and

halide ligands are bonded to the peripheral metal atoms. For example, in $[Au_{13}Ag_{12}(PPh_3)_{10}(Br)_8]^+$, two such icosahedra share a common Au vertex and 6 Br atoms bridge adjacent Ag atoms between the two icosahedra [39]. Very recently, several related Pt-centered Au—Ag supraclusters have been prepared and structurally characterized independently by Teo et al. [40] and by Kappen et al. [41]. In both of these cases the supraclusters were prepared partially from preformed clusters [40,41]:

$$[Pt(AuPPh_3)_8]^{2+} + (PPh_3)_4Ag_4Cl_4 + NaBH_4 \rightarrow [(PPh_3)_{10}Au_{12}Ag_{12}PtCl_7]Cl \quad (\text{solvent} = EtOH) \quad (44)$$

$$[Pt(H)(PPh_3)(AuPPh_3)_7]^{2+} + Ag(PPh_3)NO_3 + Cl^- \rightarrow [(PPh_3)_{10}Au_{10}Ag_{13}Pt_2Cl_7] \quad (\text{solvent} = MeOH) \quad (45)$$

Teo et al. have also reported to have prepared the Ni analog of the supracluster shown in Eq. (44), $[(PPh_3)_{10}Au_{12}Ag_{12}NiCl_7](SbF_6)$ [40,42]. These reports significantly open up the exciting area of supracluster synthesis and it is probable that many new such compounds will soon be prepared. Indeed, one can envision the synthesis of a wide variety of new clusters by combining the reactivity principles summarized above. These new materials will be very useful in the study of the physical and catalytic properties of heterometallic cluster systems.

4. Structural properties

4.1. General

The structural properties of phosphine stabilized, M—Au cluster compounds have been recently reviewed by Mingos and Watson [6]. Therefore we will only briefly mention the most important features for Pt- and Pd-centered Au clusters as determined by single-crystal X-ray diffraction. In all known $L_x—M—Au_y$ clusters the transition metal M is in the center and the L and Au atoms lie on the periphery. This has been attributed to the stronger metal–metal bonds formed by the Pt or Pd and is consistent with site preference ideas developed theoretically [6,42,43]. In cases which have another ligand such as PPh_3, halide, RNC, or CO bonded to the central metal, the clusters adopt a hemispherical geometry with the Au atoms grouped around one-half of the sphere. Several examples are $[M(CO)(AuPPh_3)_8]^{2+}$ (M = Pd or Pt) and $[Pt(PPh_3)(AuPPh_3)_6]^{2+}$ shown in Figs. 1 [15,16] and 2 [17]. Another general feature of these clusters is the predominance of triangular faces leading to centered, icosahedral based structures, although there are some examples of clusters with square faces and distorted cubic structures (see below). Finally, nearly all the $M—Au_x$ clusters are stereochemically non-rigid in the solution phase as determined by ^{31}P NMR spectroscopy. This is a consequence of the soft potential energy surface associated with geometric transformations for gold clusters [6] and

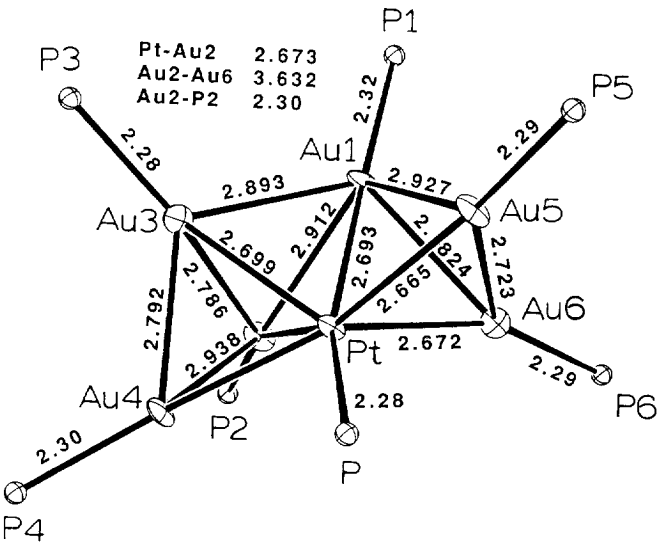

Fig. 2. ORTEP drawing of the coordination core of $[Pt(PPh_3)(AuPPh_3)_6](NO_3)_2$ with selected distances in ångströms. Average estimated standard deviations for M—M and M—P distances are 0.001 Å and 0.01 Å respectively. Reproduced with permission from the American Chemical Society, Ref. [17].

leads to the possibility of structural isomers and structural changes between solution and solid phases.

The radial M—Au bond lengths in these clusters range from 2.6 to 2.8 Å while the closest Au—Au distances are longer, ranging from 2.8 to 3.0 Å. Distances within the cluster frame of $[Pt(PPh_3)(AuPPh_3)_6]^{2+}$ are shown in Fig. 2 [17] as an example. Radial M—Au bonding is therefore more important than the weaker, peripheral Au—Au interactions which show a larger variation in distance, sometimes longer than 3 Å. The Au—PPh_3 vectors in these clusters are approximately trans to the central M atom with M—Au—P angles ranging from 165° to 180°.

4.2. Toroidal and spheroidal geometries of 16- and 18-electron clusters

The most important structural property of these clusters is the change in geometry associated with a change in the number of valence electrons from 16 to 18 as discussed in Section 2. Another example of the change from toroidal to spheroidal geometry is shown in Fig. 3 for the 16-electron cluster $[Pt(PPh_3)(AuPPh_3)_6]^{2+}$ and the 18-electron cluster $[Pt(CO)(PPh_3)(AuPPh_3)_6]^{2+}$ [17]. Most of the structures of 18-electron, spheroidal clusters can be described as M-centered, icosahedral fragments. This is best illustrated by drawing the structure as part of a centered icosahedron framework as shown in Fig. 4 [13]. The peripheral Au, Hg, and Ag atoms in these structures lie very near the vertex positions of the icosahedron, and in most cases the ligands bound to the central metal point in these directions as well. There are several 18-electron, spheroidal clusters which do not have the

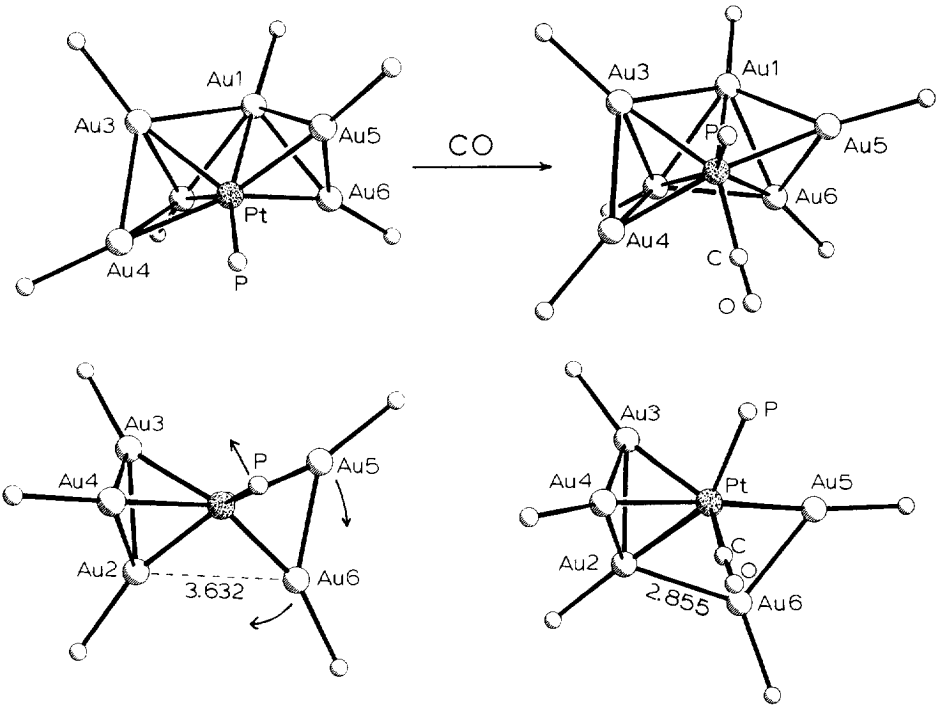

Fig. 3. PLUTO drawings of two perspectives of the cluster core of $[Pt(PPh_3)(AuPPh_3)_6]^{2+}$ and $[Pt(CO)(PPh_3)(AuPPh_3)_6]^{2-}$ showing the structural changes on the addition of CO. The lower view is along the Pt—Au1 bond, and the arrows show the major shifts in atomic positions on the addition of CO. Reproduced with permission from the American Chemical Society, Ref. [17].

icosahedral fragment geometry. Examples include $[Pt(Hg)_2(AuPPh_3)_8]^{4+}$ which has a bi-capped square-antiprismatic geometry (Fig. 5) [32], and $[Pt(C{\equiv}C{-}t\text{-}Bu)(PPh_3)(AuPPh_3)_6]^{+}$ [44] and $[Pt(H)(PPh_3)(AuPPh_3)_7]^{2+}$ [21] which have distorted cubic structures (Figs. 6 and 7). In the case of $[Pt(HgNO_3)(PPh_3)(AuPPh_3)_6]^{+}$ the geometry is between those of an icosahedral fragment and a distorted cube as shown in Fig. 7 [28]. These examples show that different spheroidal structures are possible for 18-electron clusters, although the great predominance of the centered icosahedron suggests that it is the more stable form. The non-rigid nature of these clusters in solution (see below) suggests that rapid isomerization between these different forms occurs. It is also likely that crystal packing forces are important in determining which geometry is found in the solid state.

4.3. *Structures of hydrido clusters*

The structures of hydrido Pt—Au clusters deserve special mention because of their relevance to catalytic H_2 activation. The number of such clusters has significantly

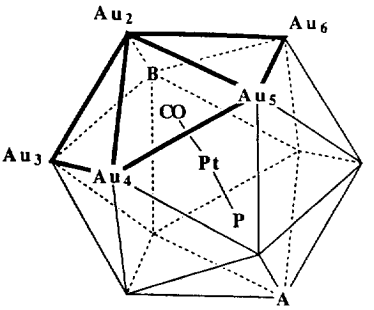

$[(CO)(PPh_3)Pt(AuPPh_3)_5]^+$

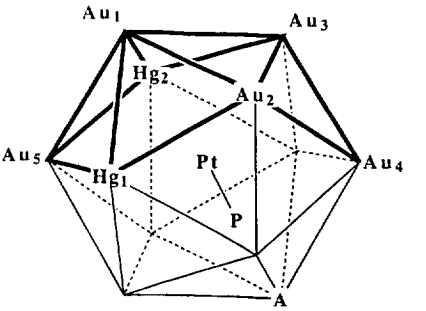

$[(PPh_3)Pt(AuPPh_3)_5(HgNO_3)_2]^+$

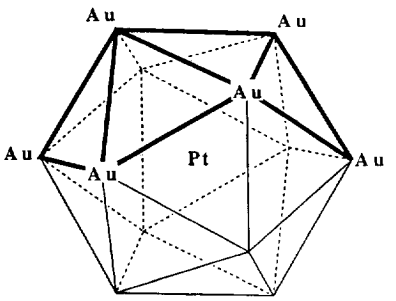

$[(CO)(PPh_3)Pt(AuPPh_3)_6]^{+2}$

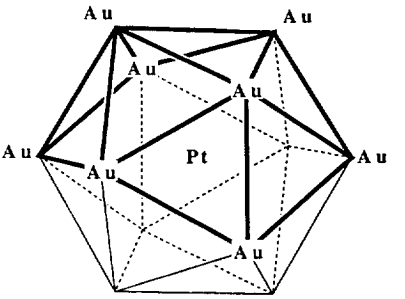

$[(CO)Pt(AuPPh_3)_8]^{+2}$

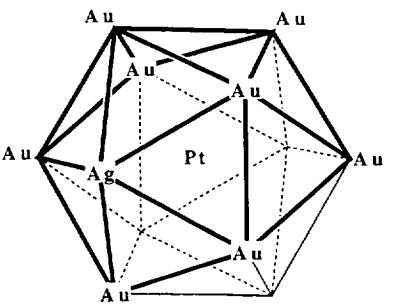

$[(CO)Pt(AuPPh_3)_8(AgNO_3)]^{+2}$

Fig. 4. Metal core geometries of several 18-electron, Pt-centered clusters shown as fragments of the centered icosahedron. The darkened lines represent bonding interactions between metal atoms. The central Pt atom is bonded to all the peripheral metals, but these bonds are not shown for the sake of clarity. Reproduced with permission from the American Chemical Society, Ref. [13].

increased during the past several years and they have an obvious importance in hydrogen activation catalysis. There are no known hydrido Pd—Au clusters although they have been implicated as undetectable intermediates in catalysis studies [3]. All

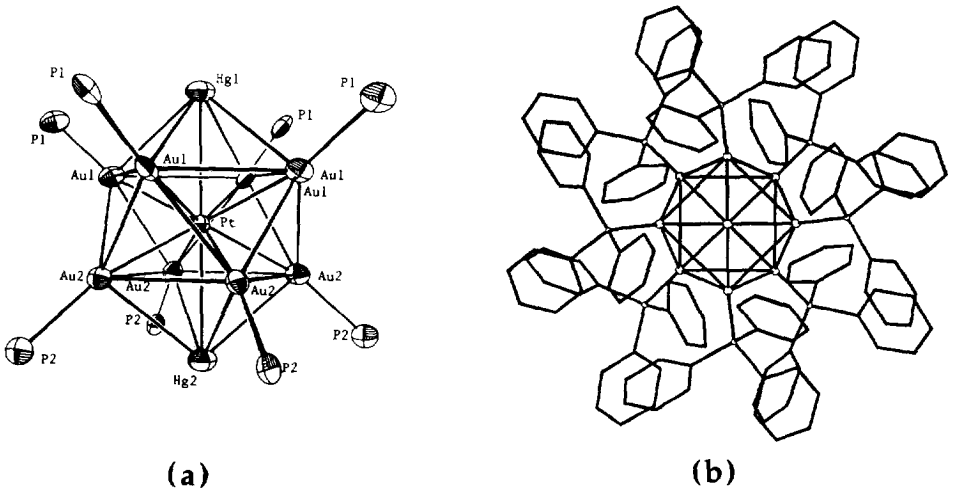

Fig. 5. Two views of the structure of $[Pt(Hg)_2(AuPPh_3)_8]^{4+}$ showing the bi-capped square-antiprismatic geometry. View (b) shows the cluster along the Hg—Pt—Hg axis. Adapted from Ref. [32].

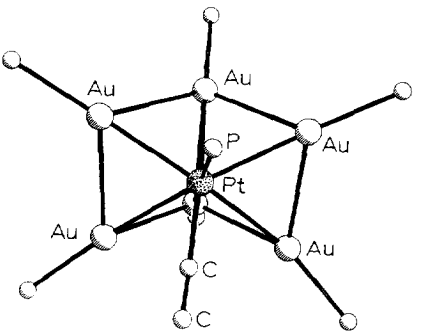

Fig. 6. PLUTO drawing of the cluster core of $[Pt(C{\equiv}C{-}t\text{-}Bu)(PPh_3)(AuPPh_3)_6]^+$. The Au, P, and C atoms lie near the corners of a distorted cube illustrating an alternative, spheroidal geometry. Reproduced with permission from the American Chemical Society, Ref. [17].

the known hydrido Pt—Au clusters are listed in Table 1. In all these clusters the hydrogen ligands are thought to be bridging between the Pt and one or two Au atoms. The evidence for this is unfortunately indirect. It is based on the absence of terminal Pt—H stretching vibrations in the IR, X-ray crystallographic structural parameters of the non-hydride atoms, NMR coupling constants, and potential energy calculations with use of Orpen's computer program [45], and by analogy to other hydrido M—Au cluster compounds [21,46]. For example, in $[Ru(dppm)_2(m\text{-}H)_2(AuPPh_3)_2]^+$ [46] and $[Ir(triphos)(Cl)(\mu\text{-}H)(AuPPh_3)_2]^+$ [47] the bridging hydrides have been directly observed by X-ray diffraction. In $[Pt(H)(PPh_3)(AuPPh_3)_7](NO_3)_2$, all the data support the placement of the hydrido ligand in a triply bridging position as shown in Fig. 8 [21]. A final comment is

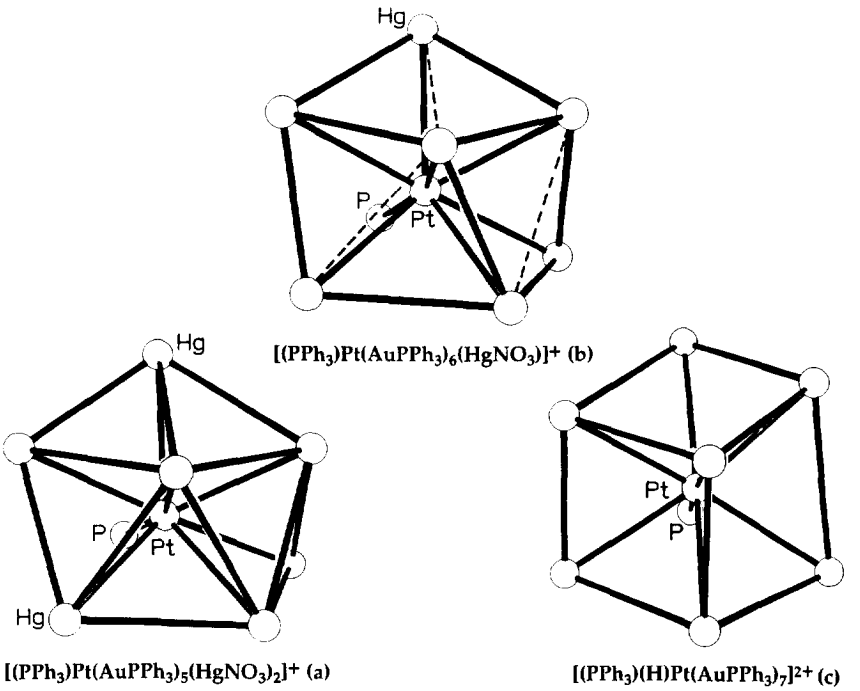

Fig. 7. PLUTO drawings of the $Pt(P)M'_7$ cluster cores of (a) $[Pt(HgNO_3)_2(PPh_3)(AuPPh_3)_5]^+$, (b) $[Pt(HgNO_3)(PPh_3)(AuPPh_3)_6]^+$ and (c) $[Pt(H)(PPh_3)(AuPPh_3)_7]^{2+}$ showing the geometry change from an icosahedral fragment to a distorted cube. The peripheral M′—M′ distances shown with broken lines in (b) are significantly elongated compared with those with full lines giving distorted, non-planar square faces. Reproduced with permission from the American Chemical Society, Ref. [28].

Table 1
Hydrido platinum–gold cluster compounds

Compound	^{1}H NMR data[a]				^{195}Pt NMR[b] δ (ppm)	Ref.
	δ (ppm)	J(H—Pt)	^3J(H—P)	^2J(H—P)		
$[Pt(H)(PPh_3)(AuPPH_3)_6]^+$	0.34	687	18.3	9.2	−5035	[31]
$[Pt(H)(PPh_3)(AuPPh_3)_7]^{2+}$	2.26	537	16.6	6.6	−5425	[21]
$[Pt(H)(SnCl_3)(AuPPh_3)_7]^+$	2.75	680	16.2	—	−5634	[31]
$[Pt(H)(AuPPh_3)_8]^+$	5.4	705	14.3	—	−5673	[31]
$[Pt(H)_2(AuPPh_3)_8]^{2-}$	3.9[c]	645	13.7	—	−5994	[2,3]
$[Pt(H)(Ag)(AuPPh_3)_8]^{2-}$	1.74	716	12.5	—	−6036	[34]
$[Pt(H)(Ag)_2(AuPPh_3)_8]^{3-}$	—[d]	611	—[d]	—	−6348	[34]

[a] CD_2Cl_2, ambient temperature, reference to tetramethylsilane (TMS).
[b] CH_2Cl_2, ambient temperature, reference to K_2PtCl_6 in D_2O.
[c] Recorded at −30 °C.
[d] Not reported.

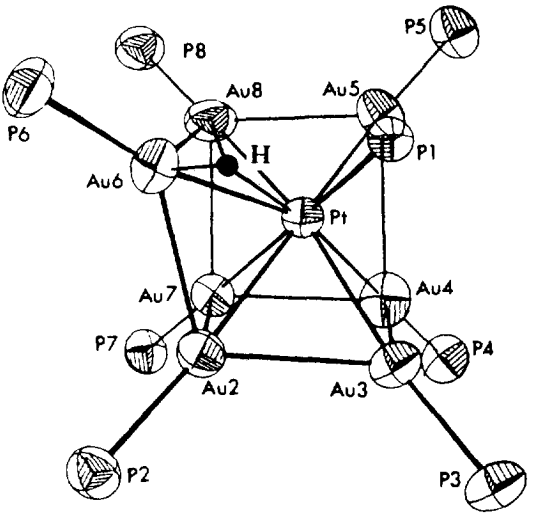

Fig. 8. ORTEP drawing of the cluster core of $[Pt(H)(PPh_3)(AuPPh_3)_7]^{2+}$ showing the most probable position for the hydrido ligand. Adapted from Ref. [21].

needed on fluxionality in these clusters. It has already been pointed out that most $M-Au_x$ clusters are fluxional in solution on the NMR timescale. In all the hydrido Pt—Au clusters the different geometric sites for AuP in the crystalline state are equilibrated in solution at room temperature by fast fluxionality. In effect, the H ligand(s) are rapidly scrambling around the metal framework of the cluster.

4.4. *Structures of supraclusters*

The structures of the 25-metal-atom, Pt—Au—Ag supraclusters $[(PPh_3)_{10}Au_{12}Ag_{12}PtCl_7]^+$ [40] and $[(PPh_3)_{10}Au_{10}Ag_{13}Pt_2Cl_7]$ [41] are similar to those of the 25-metal-atom Au—Ag supraclusters prepared by Teo and co-workers [36] with the Pt atoms occupying the centered positions of the vertex-shared icosahedral units. The structures of these two new supraclusters are shown in Fig. 9. The drawing of $[(PPh_3)_{10}Au_{10}Ag_{13}Pt_2Cl_7]$ shown in Fig. 10 [41] better illustrates the vertex-shared, bi-icosahedral framework. The basic difference between these two supraclusters is that in $[(PPh_3)_{10}Au_{12}Ag_{12}PtCl_7]^+$ a A atom occupies the position shared between the two icosahedra and one of the icosahedra is Au centered (disordered with the other Pt-centered icosahedron), while in $[(PPh_3)_{10}Au_{10}Ag_{13}Pt_2Cl_7]$ the two icosahedra are Pt centered and a Ag atom occupies the shared position. The structural details of Au—Ag supraclusters and a rationalization of their structures by electron counting rules has been recently reviewed [6,48] and the Pt—Au—Ag analogs are described in the review by Teo in this journal [49]. The Pt-centered, vertex-shared icosahedra in these supraclusters each have 18 valence electrons, and therefore the compounds are expected to be unreactive with nucleophiles. They have been shown to be inactive for dihydrogen activation (see below).

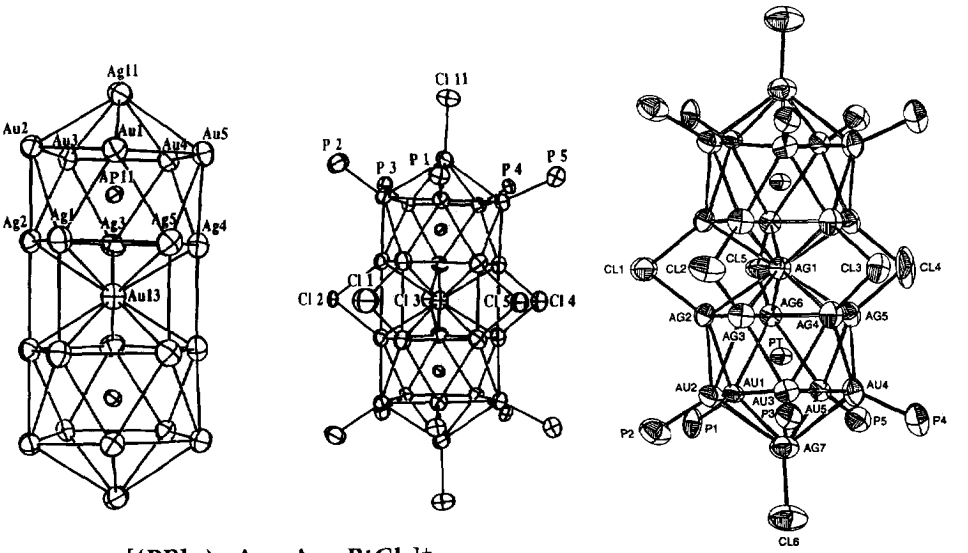

$[(PPh_3)_{10}Au_{12}Ag_{12}PtCl_7]^+$ $[(PPh_3)_{10}Au_{10}Ag_{13}Pt_2Cl_7]$

Fig. 9. Structures of the two Pt-centered, vertex-shared, icosahedral supraclusters $[(PPh_3)_{10}Au_{12}Ag_{12}PtCl_7]^+$ and $[(PPh_3)_{10}Au_{10}Ag_{13}Pt_2Cl_7]$. Both structures contain crystallographic mirror planes passing through the Cl atoms and the atom shared between the icosahedral units. In the former compound, a Pt and an Au atom are equally disordered between the two icosahedal centers related by the mirror plane. Adapted from Refs. [40] and [41].

5. Spectroscopic properties

Most of the spectroscopic studies of M—Au cluster compounds have been done as part of cluster characterization. The primary techniques used are NMR, IR, and UV–visible absorption spectroscopy, inductively coupled plasma atomic emission spectroscopy (ICPAES), and FABMS. Many of the Pt—Au clusters have also been studied by X-ray photoelectron spectroscopy (XPS) [50]. ICPAES is very useful as an analytical [51,52] tool but will not be discussed further here. IR spectroscopy has been used primarily to determine the bonding mode or lack of bonding of ligands such as NO_3^-, CO, and RNC but otherwise has not proved particularly useful. For example, many attempts have been made in solid and solution phases at different temperatures to observe metal–hydride stretches. All of these attempts have failed with Pt—Au hydrido clusters, although weak vibrations assigned to bridging modes have been observed for some Ir—Au hydrido clusters by Bianchini et al. [47] and Albinati et al. [53].

5.1. UV–visible absorption spectroscopy

UV–visible absorption spectra have been recorded in the solution phase for a number of M—Au cluster compounds by Schoondergang [52] and are listed in

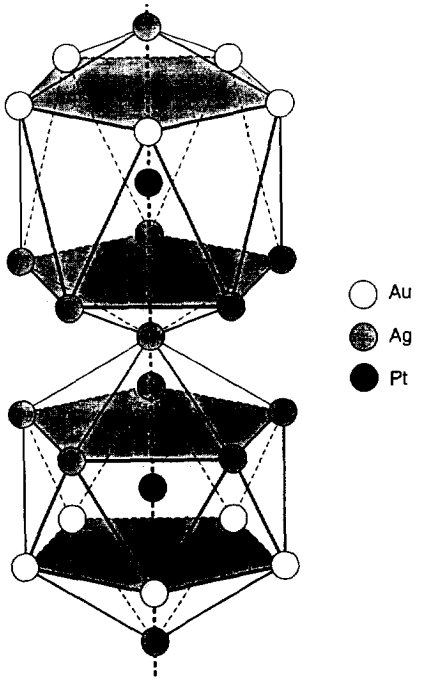

Fig. 10. Vertex-shared, bi-icosahedral metal framework of the supracluster $[(PPh_3)_{10}Au_{10}Ag_{13}Pt_2Cl_7]$. Adapted from Ref. [41].

Table 2. With few exceptions, 16-electron clusters appear dark colored (brown to black) while 18-electron clusters are lighter and range in color from yellow–orange to deep red. The spectra of 16-electron clusters generally show reasonably well-resolved absorption bands in the 250–600 nm range while the spectra of 18-electron clusters usually consist of broader, less-defined shoulder absorptions. Absorption spectra of the 16- and 18-electron clusters $[Pt(AuPPh_3)_8]^{2+}$ and $[Pt(CO)(AuPPh_3)_8]^{2+}$ are shown in Fig. 11 [52]. These differences are general and can be used to distinguish between 16- and 18-electron clusters, although there are some exceptions.

5.2. *Fast atom bombardment mass spectroscopy*

FABMS is extremely useful in determining the molecular formula of the parent cluster [18]. Assignment of the cluster fragments provides additional information about cluster composition. As an example, the FABMS spectrum for the supracluster $[(PPh_3)_{10}Au_{10}Ag_{13}Pt_2Cl_7]$ is shown in Fig. 12 [41]. Note that the most abundant peak in the 4500–7000 mass range is due to the parent molecular ion. This is a convincing example of the usefulness of this technique in cluster characterization. Indeed, in many cases it provides the best information about the nature of a new cluster because X-ray quality crystals are often impossible to obtain and NMR gives

Table 2
Absorption maxima of some Pt–Au and Pd–Au cluster compounds [52]

Compound	NE[a]	Band positions λ_{max} (nm) (log ε_{max})[b]
$[Au(AuPPh_3)_8]^{3+}$	16	443 (4.21), 375 (sh), 352 (sh), 314 (4.78)
$[Pt(AuPPh_3)_8]^{2-}$	16	515 (sh), 482 (3.93), 431 (4.27), 400 (4.25), 354 (4.71)
$[Pd(AuPPh_3)_8]^{2+}$	16	518 (3.79), 464 (4.10), 413 (4.30), 347 (4.76), 313 (sh), 298 (4.80)
$[Pt(PPh_3)(AuPPh_3)_6]^{2-}$	16	460 (3.88), 400 (4.07), 330 (4.75)
$[Pt(Ag)(AuPPh_3)_8]^{3+}$	16	490 (3.80), 431 (4.34), 382 (sh), 355 (sh), 331 (4.81)
$[Pt(CuCl)(AuPPh_3)_8]^{2+}$	16	528 (3.79), 464 (4.12), 413 (4.32), 347 (4.78), 312 (sh), 298 (4.82)
$[Pt(H)(PPh_3)(AuPPh_3)_7]^{2+}$	18	387 (sh), 330 (sh), 300 (sh)
$[Pt(PPh_3)(AuPPh_3)_7]^{+}$	18	478 (4.18), 390 (4.60), 329 (4.77), 310 (4.90), 290 (4.97)
$[Pt(CO)(AuPPh_3)_8]^{2+}$	18	460 (sh), 433 (4.13), 330 (sh), 280 (4.95)
$[Pt(CO)(Ag)(AuPPh_3)_8]^{3-}$	18	445 (4.18), 416 (4.24), 385 (4.24), 328 (sh), 307 (sh)
$[Pt(CO)(CuCl)(AuPPh_3)_8]^{2+}$	18	454 (4.18), 425 (4.18), 314 (4.94), 302 (4.96)
$[Pt(CO)(AgCl)_2(AuPPh_3)_7]^{-}$	18	440 (4.16), 403 (4.22), 374 (4.22), 343 (sh), 308 (4.91), 292 (4.94)
$[Pt(CO)(CuCl)_2(AuPPh_3)_7]^{+}$	18	454 (4.04), 418 (4.06), 322 (sh), 292 (4.91)
$[Pt(CO)(AuCl)_2(AuPPh_3)_7]^{+}$	18	454 (sh), 412 (4.22), 373 (sh), 307 (5.00)
$[Pt(CO)(AuCl)(AuPPh_3)_7]^{+}$	18	453 (sh), 413 (4.20), 372 (sh), 306 (4.98)
$[Pt(PPh_3)(AuCl)_3(AuPPh_3)_6]$	18	480 (3.84), 421 (4.22), 347 (sh), 306 (sh, 4.84)

[a] NE, number of cluster valence electrons.
[b] Extinction coefficients in parentheses given as $\log[\varepsilon_{max}(dm^3\ mol^{-1}\ cm^{-1})]$.

only a general idea about the number and type of phosphine ligands. The use of FABMS in M–Au cluster chemistry has been reviewed previously [6] and will not be discussed further here.

5.3. Nuclear magnetic resonance spectroscopy

$^{31}P(^1H)$ NMR provides the quickest method for the identification of known clusters and data for many Pd–Au and Pt–Au cluster compounds are given in Table 3. There are no overall trends in ^{31}P chemical shift or coupling constant values except when comparing a series of closely related clusters. For example, an increase in Pt coordination number will generally decrease P–Pt coupling constants. The ^{31}P NMR spectra of most M–Au clusters are greatly simplified because of fast fluxional behavior as previously mentioned. This phenomenon has been discussed in detail in several recent reviews [6–9]. ^{195}Pt NMR, with selective ^{31}P and ^1H decoupling, has proved very useful in determining the number of phosphine ligands (Pt–^{31}P coupling pattern), the presence and number of hydrido ligands (Pt–^1H coupling pattern), the presence and number of other spin active metals such as Ag and Hg, and the number of valence electrons (chemical shift value). ^{195}Pt NMR chemical shift values for many Pt–Au clusters are given in Table 3 and there is a general trend with electron count. Pt-centered clusters with 18 valence

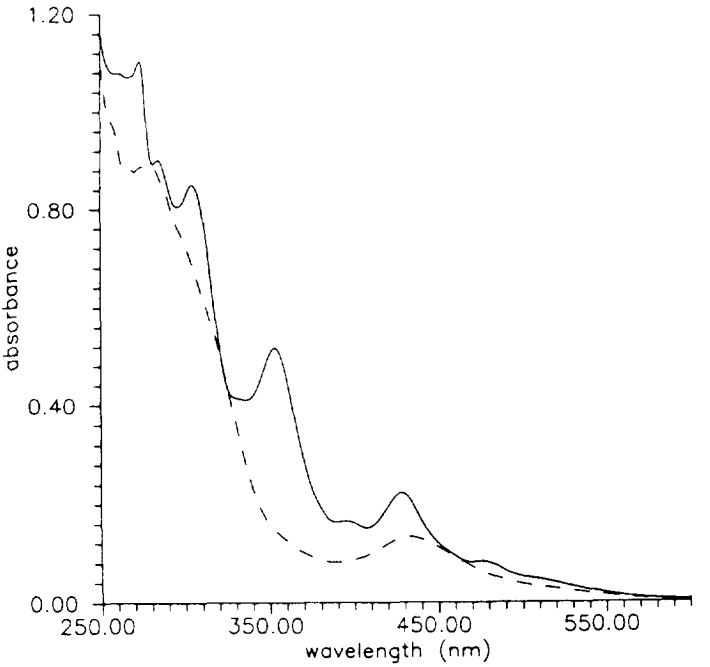

Fig. 11. Absorption spectra of $[Pt(AuPPh_3)_8](NO_3)_2$ (—) and $[Pt(CO)(AuPPh_3)_8](NO_3)_2$ (---) recorded with use of CH_2Cl_2 as solvent. Adapted from Ref. [52].

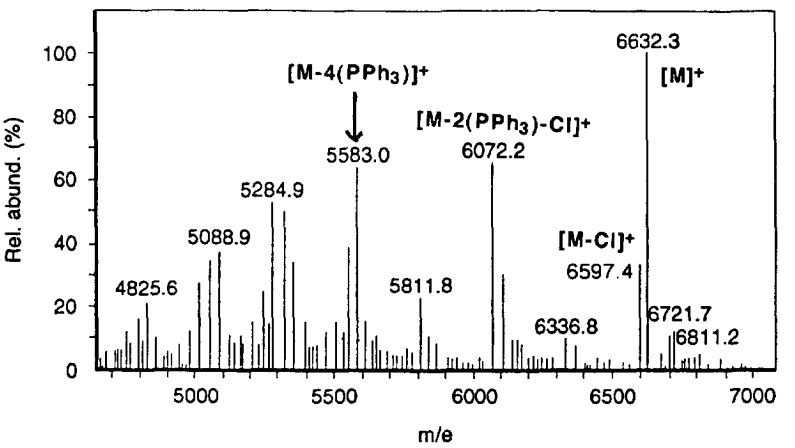

Fig. 12. Low resolution positive ion FABMS spectrum of $[(PPh_3)_{10}Au_{10}Ag_{13}Pt_2Cl_7]$ in the 4500–7000 mass range. Some of the masses are assigned to molecular fragments as indicated where M is the parent supracluster $[(PPh_3)_{10}Au_{10}Ag_{13}Pt_2Cl_7]$ which has a molecular weight of 6633.2. Reproduced with permission from the American Chemical Society, Ref. [41].

Table 3
^{31}P and ^{195}Pt nuclear magnetic resonance data for $Pt-Au_x$ and $Pd-Au_x$ cluster compounds

MAu_x cluster	δ $^{31}P\{^1H\}$[a]		$^2J(Pt-P)$	$^1J(Pt-P)$	$^3J(P-P)$	$^3J(M'-P)$[b]	δ ^{195}Pt	Ref.
$PtAu_2$								
$[Pt(NO_3)(PPh_3)_2(AuPPh_3)_2]^{+c}$	22.6 (s)	22.8 (s)	804	2502				[18]
$[Pt(Cl)(PEt_3)_2(AuPPh_3)_2]^{+c}$	42.0 (t)	35.7 (t)	792	2197	≈4			[19b]
$PtAu_3$								
$[Pt(PPh_3)_2(AuPPh_3)_3]^{+c}$	60.2 (q)	47.3 (t)	505	3673	44			[13]
$[Pt(CO)(PPh_3)_2(AuPPh_3)_3]^{+c}$	32.9 (q)	45.6 (t)	480	2633	38.5			[13]
$PtAu_4$								
$[Pt(PPh_3)_2(AuPPh_3)_4]^{2+c}$	53.9 (p)	44.0 (t)	377	3234	47.6			[13]
$[Pt(dppe)(AuPPh_3)_4]^{2+c}$	82.2 (p)	50.7 (t)	363	3098	47.6			[13]
$[Pt(I)(PPh_3)(AuPPh_3)_4]^{+c}$	57.6 (p)	43.4 (d)	498	4131	44.0			[13]
$[Pt(I)(dppe)(AuPPh_3)_4]^{+d}$	76.6 (p)	50.7 (t)	324	3236	45.7			[13]
$PtAu_5$								
$[Pt(CO)(PPh_3)(AuPPh_3)_5]^{+c}$	52.0 (sx)	47.9 (d)	448	2808	32			[17]
$[Pt(HgNO_3)_2(PPh_3)(AuPPh_3)_5]^{+c}$	54.9 (sx)	53.1 (d)	390	3258	39.7	604		[13]
$[Pt(HgCl)_2(PPh_3)(AuPPh_3)_5)^{+c}$	58.0 (sx)	51.9 (d)	386	3042	41.5	479		[13]
$[Pt(HgBr)_2(PPh_3)(AuPPh_3)_5]^{+c}$	58.8 (sx)	51.5 (d)	385	3043	40.3	473		[13]
$[Pt(HgI)_2(PPh_3)(AuPPh_3)_5]^{+c}$	60.3 (sx)	50.8 (d)	385	3036	42.1	414		[13]
$[Pt(HgCo(CO)_4)_2(PPh_3)(AuPPh_3)_5]^{+c}$	56.3 (sx)	48.4 (d)	435	2644	36.6	435		[28]
$PtAu_6$								
$[Pt(PPh_3)(AuPPh_3)_6]^{e}$	79.2 (m)	45.8 (d)	533		28.3			[52]
$[Pt(PPh_3)(AuPPh_3)_6]^{2+c}$	62.3 (sp)	50.3 (d)	413	3766	30		−4245	[17]
$\{Pt[P(p\text{-}OMePh)_3][Au(p\text{-}OMePh)_3]_6\}^{2+c}$	54.8 (sp)	46.6 (d)	394	3100	33			[52]
$[Pt(CO)(PPh_3)(AuPPh_3)_6]^{2+f}$	47.3 (sp)	48.0 (d)	385	2469	28			[17]
$[Pt(C{\equiv}CPh)(PPh_3)(AuPPh_3)_6]^{+c}$	59.4 (sp)	43.0 (d)	437		40			[17]
$[Pt(C{\equiv}C\text{-}t\text{-}Bu)(PPh_3)(AuPPh_3)_6]^{+c}$	59.0 (sp)	42.5 (d)	444	2154	41			[44]
$[Pt(H)(PPh_3)(AuPPh_3)_6]^{+c}$	68.0 (sp)	48.2 (d)	457	2583	37			[27]
$[Pt(Br)(PPh_3)(AuPPh_3)_6]^{+c}$	60.8 (sp)	48.3 (d)	439	3667	31.7			[13]
$[Pt(I)(PPh_3)(AuPPh_3)_6]^{+c}$	56.8 (sp)	45.4 (d)	493	3379	36.6			[13]
$[Pt(CN)(PPh_3)(AuPPh_3)_6]^{+c}$	59.2 (sp)	44.6 (d)	415	2222	41.5			[13]

$[Pt(P(OMe)_3)_2(AuPPh_3)_6]^{2+c}$	157 (sp)	49.0 (t)	362	4205	55.1			[13]
$\{Pt[P(OCH_2)_3CCH_3]_2(AuPPh_3)_6\}^{2+c}$	171.1 (sp)	49.2 (t)	366	4107	57.5			[13]
$[Pt(AgNO_3)_3(PPh_3)(AuPPh_3)_6]^{e}$	51.5 (m)	53–58 (br)	440	2600	80		−6349	[52]
$[Pt(HgNO_3)(PPh_3)(AuPPh_3)_6]^{+f}$	60.5 (sp)	50.5 (d)	462	3070	31.8	655		[28]
$[Pt(HgCl)(PPh_3)(AuPPh_3)_6]^{+f}$	65.4 (sp)	49.7 (d)	468	2813	35.5	566		[28]
$[Pt(HgBr)(PPh_3)(AuPPh_3)_6]^{+f}$	65.3 (sp)	49.3 (d)	470	2830	35.4	564		[28]
$[Pt(HgI)(PPh_3)(AuPPh_3)_6]^{+f}$	65.8 (sp)	49.0 (d)	471	2813	35.4	544		[28]
$[Pt(HgCo(CO)_4)(PPh_3)(AuPPh_3)_6]^{+f}$	65.4 (sp)	48.4 (d)	480	2580	35.5	480		[28]
$PtAu_7$								
$[Pt(PPh_3)(AuPPh_3)_7]^{+c}$	77.0 (o)	49.3 (d)	492	2411	33		−4916	[52]
$[Pt(H)(PPh_3)(AuPPh_3)_7]^{2+c}$	61.0 (o)	47.5 (d)	414	2300	34		−5425	[21]
$[Pt(H)(PPh_3)(AuCl)(AuPPh_3)_6]^{+c}$	50.0 (sp)	46.6 (d)	374		30.3			[26]
$[Pt(H)(PPh_3)(AuBr)(AuPPh_3)_6]^{+c}$	54.2 (sp)	46.6 (d)	378		29.1			[26]
$[Pt(H)(PPh_3)(AuI)(AuPPh_3)_6]^{+c}$	55.2 (sp)	46.7 (d)	379	2735	27.6		−5541	[26]
$[Pt(H)(SnCl_3)(AuPPh_3)_7]^{+c}$		51.1 (s)	445			372, 389	−5634	[27]
$[Pt(CO)(AgNO_3)_2(AuPPh_3)_7]^{+c}$		58.0 (t)	395			17.4	−5908	[33,52]
$[Pt(CO)(AgCl)_2(AuPPh_3)_7]^{+c}$		56.4 (t)	395			15.8		[33]
$[Pt(CO)(CuCl)_2(AuPPh_3)_7]^{+c}$		55.3 (s)	377				−5904	[33,52]
$[Pt(HgNO_3)_2(AuPPh_3)_7]^{+c}$		57.2 (s)	471			580		[32]
$PtAu_8$								
$[Pt(AuPPh_3)_8]^{2+c}$		55.4 (s)	497				−4528	[21]
$\{Pt[AuP(p\text{-}OMePh)_3]_8\}^{2+c}$		51.5 (s)	496					[52]
$\{Pt[AuP(p\text{-}MePh)_3]_8\}^{2+c}$		53.2 (s)	495					[3]
$[Pt(AuPPh_3)_8]^{e}$		52.8 (s)	564					[52]
$[Pt(H)(AuPPh_3)_8]^{+c}$		52.1 (s)	452				−5673	[27]
$[Pt(H)_2(AuPPh_3)_8]^{2+c}$		51.5 (br s)	380				−5994	[2]
$[Pt(CO)(AuCl)(AuPPh_3)_7]^{+c}$		52.4 (s)	379					[54]
$[Pt(CO)(AuBr)(AuPPh_3)_7]^{+c}$		51.7 (s)	384					[54]
$[Pt(CO)(AuI)(AuPPh_3)_7]^{+c}$		51.6 (s)	384				−5535	[54]
$[Pt(CO)(AuOR)(AuPPh_3)_7]^{+c,g}$		52.3 (s)	379				−5678	[54]
$[Pt(CO)(AuCNR)(AuPPh_3)_7]^{2+c,h}$		53.2 (s)	372				−5622	[15]
$[Pt(CO)(AuCNR')(AuPPh_3)_7]^{2+c,h}$		52.8 (s)	373				−5625	[55]
$[Pt(CO)(AuCN)_2(AuPPh_3)_6]^{c}$		52.4 (s)	386				−5822	[31]
$[Pt(CNR)(AuCNR)(AuPPh_3)_7]^{2+c,h}$		51.9 (s)	379				−5424	[15]
$[Pt(CNR)(AuCNR')(AuPPh_3)_7]^{2+c,h}$		51.5 (s)	380				−5423	[55]
$[Pt(CO)(AuPPh_3)_8]^{2+c}$		51.3 (s)	391				−5457	[14,15]

Table 3 (*continued*)

MAu_x cluster	δ $^{31}P(^1H)$[a]	^2J(Pt−P)	^1J(Pt−P)	^3J(P−P)	^3J(M′−P)[b]	δ ^{195}Pb	Ref.
$[Pt(CNR)(AuPPh_3)_8]^{2+}$ [c,h]	50.4 (s)	400				−5271	[15]
$[Pt(CNR')(AuPPh_3)_8]^{2+}$ [c,h]	49.8 (s)	403				−5287	[55]
$[Pt(CNR')(AuCNR)(AuPPh_3)_7]^{2+}$ [c,h]	51.1 (s)	383				−5435	[55]
$[Pt(CNR')(AuCNR')(AuPPh_3)_7]^{2+}$ [c,h]	51.1 (s)	383				−5435	[55]
$[Pt(CuCl)(AuPPh_3)_8]^{2+}$ [c]	56 (br s)	445				−4364	[33]
$[Pt(CuMeCN)(AuPPh_3)_8]^{3+}$ [c]	56.9 (s)	441					[52]
$[Pt(CO)(CuCl)(AuPPh_3)_8]^{2+}$ [c]	53.5 (s)	361				−5738	[33]
$[Pt(CO)(CuMeCN)(AuPPh_3)_8]^{3+}$ [c]	54.5 (s)	357					[52]
$[Pt(CO)(CuCl)(AuCl)(AuPPh_3)_7]^{+}$ [c]	52.5 (s)	355					[52]
$[Pt(CO)(CuCl)(AuI)(AuPPh_3)_7]^{+}$ [c]	52.7 (s)	357					[52]
$[Pt(AgNO_3)(AuPPh_3)_8]^{2+}$ [i]	57 (br)	453			19	−4376	[14]
$[Pt(AgCl)(AuPPh_3)_8]^{2+}$ [c]	56.5 (d)	453			19		[33]
$[Pt(AgMeCN)(AuPPh_3)_8]^{3+}$ [c]	57.4 (d)	452			20		[52]
$[Pt(CO)(AgNO_3)(AuPPh_3)_8]^{2+}$ [i]	54.7 (d)	366			17	−5688	[14]
$[Pt(CO)(AgCl)(AuPPh_3)_8]^{2+}$ [c]	54.0 (d)	370			17		[33]
$[Pt(CO)(AgMeCN)(AuPPh_3)_8]^{3+}$ [c]	55.2 (d)	363			15		[52]
$[Pt(CO)(AgNO_3)(AuCNR)(AuPPh_3)_7]^{2+}$ [h,i]	54.4 (d)	355			16		[55]
$[Pt(CO)(AgNO_3)(AuCNR')(AuPPh_3)_7]^{2+}$ [h,i]	54.1 (d)	362			16		[55]
$[Pt(CO)(AgCl)(AuCl)(AuPPh_3)_7]^{+}$ [c]	53.1 (d)	362			16.5		[52]
$[Pt(CNR)(AgNO_3)(AuPPh_3)_8]^{2+}$ [h,j]	51.4 (br d)	350					[55]
$[Pt(CNR)(AgNO_3)(AuCNR)(AuPPh_3)_7]^{2+}$ [h,i]	52.7 (br d)	365			12		[55]
$[Pt(CNR)(AgNO_3)(AuCNR')(AuPPh_3)_7]^{2+}$ [h,i]	52.4 (br d)	360			12		[55]
$[Pt(H)(AgNO_3)(AuPPh_3)_8]^{+}$ [k]	56.2 (d)	410			21	−6036	[34]
$[Pt(H)(AgNO_3)(AuPPh_3)_8]^{+}$ [c]	54.7 (d)	412			19		[34]
$[Pt(H)(AgCl)(AuPPh_3)_8]^{+}$ [k]	55.3 (d)	414			18		[34]
$[Pt(H)(AgCl)(AuPPh_3)_8]^{+}$ [c]	54.0 (d)	411			17		[34]
$[Pt(H)(AgNO_3)_2(AuPPh_3)_8]^{+}$ [k]	60.0 (d)	406			20		[34]
$[Pt(H)(AgNO_3)_2(AuPPh_3)_8]^{+}$ [c]	58.6 (d)	407			19	−6348	[34]
$[Pt(H)(AgCl)_2(AuPPh_3)_8]^{+}$ [c]	57.6 (d)	406			16		[34]
$[Pt(HgNO_3)_2(AuPPh_3)_8]^{2+}$ [c]	58.4 (s)	406			471	−6301	[32]
$[Pt(HgCl)_2(AuPPh_3)_8]^{2+}$ [c]	57.8 (s)	395			356		[32]
$[Pt(HgNO_3)_2(AuNO_3)(AuPPh_3)_7]^{+}$ [c]	58.2 (s)	394			545	−6761	[32]
$[Pt(HgCl)_2(AuCl)(AuPPh_3)_7]^{+}$ [c]	57.3 (s)	386			406	−6560	[32]

$PtAu_9$						
$[Pt(AuPEt_3)_9]^{3+}$ [f]	57.0 (br)	407				[25]
$[Pt(CO)(AuPEt_3)_9]^{3+}$ [f]	51.6 (s)	338				[25]
$[Pt(CN)(AuCN)(AuPPh_3)_8]^{+}$ [c]	50.2 (d)	360			−5507	[31]
$[Pt(PPh_3)(AuCl)_3(AuPPh_3)_6]$ [c]	38.8 (m)		2614	90		[26]
$[Pt(PPh_3)(AuCl)_3(AuPPh_3)_6]$ [c]	41.4 (s)	288				[26]
$[Pt(PPh_3)(AuCl)_3(AuPPh_3)_6]$ [c]	43.2 (d)	325		90		[26]
$[Pt(PPh_3)(AuBr)_3(AuPPh_3)_6]$ [c]	38.1 (m)		2614	82		[26]
$[Pt(PPh_3)(AuBr)_3(AuPPh_3)_6]$ [c]	42.3 (s)	286				[26]
$[Pt(PPh_3)(AuBr)_3(AuPPh_3)_6]$ [c]	43.3 (d)	345		82		[26]
$[Pt(PPh_3)(AuI)_3(AuPPh_3)_6]$ [c]	37.6 (m)		2700	90		[26]
$[Pt(PPh_3)(AuI)_3(AuPPh_3)_6]$ [c]	43.0 (s)	290				[26]
$[Pt(PPh_3)(AuI)_3(AuPPh_3)_6]$ [c]	43.7 (d)	341		90		[26]
$[Pt(PPh_3)(AuSCN)_3(AuPPh_3)_6]$ [c]	47.6 (m)		2570	83		[26]
$[Pt(PPh_3)(AuSCN)_3(AuPPh_3)_6]$ [c]	42.2 (s)	293				[26]
$[Pt(PPh_3)(AuSCN)_3(AuPPh_3)_6]$ [c]	43.0 (d)	351		83		[26]
$PtAu_{10}$						
$[Pt(AuPEt_3)_{10}]^{2+}$ [f]	51.4 (s)	354				[25]
$PdAu_6$						
$[Pd(PPh_3)(AuPPh_3)_6]^{2+}$ [c]	59.8 (sp) 47.5 (d)			31		[16,20]
$\{Pd[P(OCH_2)_3CCH_3]_2(AuPPh_3)_6\}^{2+}$ [c]	185.1 (sp) 44.3 (t)			56		[16]
$PdAu_8$						
$[Pd(AuPPh_3)_8]^{2+}$ [c]	48.8 (s)					[16,20]
$[Pd(CO)(AuPPh_3)_8]^{2+}$ [c]	44.5 (s)					[16,20]
$[Pd(HgNO_3)_2(AuPPh_3)_8]^{2+}$ [f]	45.0 (s)				643	[29]
$PdAu_9$						
$[Pd(I)(AuI)_2(AuPPh_3)_7]$ [c]	45.4 (br)					[30]
$PdAu_{10}$						
$[Pd(AuCl)_3(AuPPh_3)_7]^{+}$ [c]	44.6 (br)					[30]
$[Pd(AuBr)_3(AuPPh_3)_7]^{+}$ [c]	46 (br)					[30]
$[Pd(CO)(AuCl)_3(AuPPh_3)_7]^{+}$ [c]	44.3 (s)					[30]
$[Pd(CO)(AuBr)_3(AuPPh_3)_7]^{+}$ [c]	40 (br) 45 (br)					[30]

Table 3 (*continued*)

MAu_x cluster	δ $^{31}P(^1H)$[a]	^2J(Pt–P)	^1J(Pt P)	^3J(P–P)	^3J(M′–P)[b]	δ ^{195}Pb	Ref.
$PdAu_{11}$							
$[Pd(AuCl)_3(AuPPh_3)_8]$[c]	40.5 (s) 50.7 (s)						[30]
$[Pd(AuCN)_3(AuPPh_3)_8]$[c]	44.8 (s)						[30]
Supracluster							
$[Pt_2Ag_{13}(AuPPh_3)_{10}Cl_7]$	59.6 (d)	520					[41]

[a] Phosphorus chemical shifts are listed parts per million relative to internal standard TMP with positive shifts downfield. The shifts are listed in the order they appear in the formula, i.e. P– Pt preceeds P–Au; symbols in parentheses refer to coupling pattern and are as follows: br, broad; m, multiplet; s, singlet; d, doublet; t, triplet; q, quartet; p, pentet; sx, sextet; sp, septet; o, octet.

[b] M′ refers to the metals Ag, Sn, and Hg, and ^3J(M′ P) values are listed in the order the M′ atoms appear in the formula.

[c] CH_2Cl_2, ambient temperature.

[d] 1,1,2-trichloroethane, 75 °C.

[e] Toluene, ambient temperature.

[f] Acetone, ambient temperature.

[g] R=H or CH_3.

[h] R=*i*-Pr, R′=*t*-Bu.

[i] Ethanol, 56 °C.

[j] Ethanol, ambient temperature.

[k] CD_3OD, ambient temperature.

electrons have ^{195}Pt chemical shifts upfield of ≈ -5400 ppm whereas 16-electron clusters have values downfield of ≈ -4500 ppm [34]. ^{195}Pt NMR spectra of $[Pt(H)(Ag)(AuPPh_3)_8]^{2+}$ are shown in Fig. 13 [34]. This is a good example which illustrates the power of ^{195}Pt NMR in cluster characterization. The chemical shift is centered at -6036 ppm indicative of an 18-electron cluster. The separate doublet patterns ($^1J(Pt-^{107}Ag)=425$ Hz and $^1J(Pt-^{109}Ag)=487$ Hz) in the $^{195}Pt(^{31}P,^1H)$ spectrum (Fig. 13(a)) indicate the presence of one Ag atom (^{107}Ag and ^{109}Ag isotopes are spin active), and the doublet pattern ($^1J(Pt-^1H)=716$ Hz) in the $^{195}Pt(^{31}P)$ spectrum (Fig. 13(b)) indicates the presence of one H ligand. The presence of eight $AuPPh_3$ units bonded to the Pt atom gives rise to a nonet caused by $^2J(Pt-^{31}P)$, but because the $^1J(Pt-Ag)$ couplings give rise to a doublet structure and are in the same range as this $^2J(Pt-^{31}P)$, the overall $^{195}Pt(^1H)$ spectrum (Fig. 13(c)) results in an even multiplet that can be simulated (Fig. 13(d)) for eight P atoms with $^2J(Pt-^{31}P)=412$ Hz.

^1H NMR of hydrido Pt–Au clusters has been useful in the direct detection of the hydrido ligand. Data for some typical clusters are shown in Table 1. The most

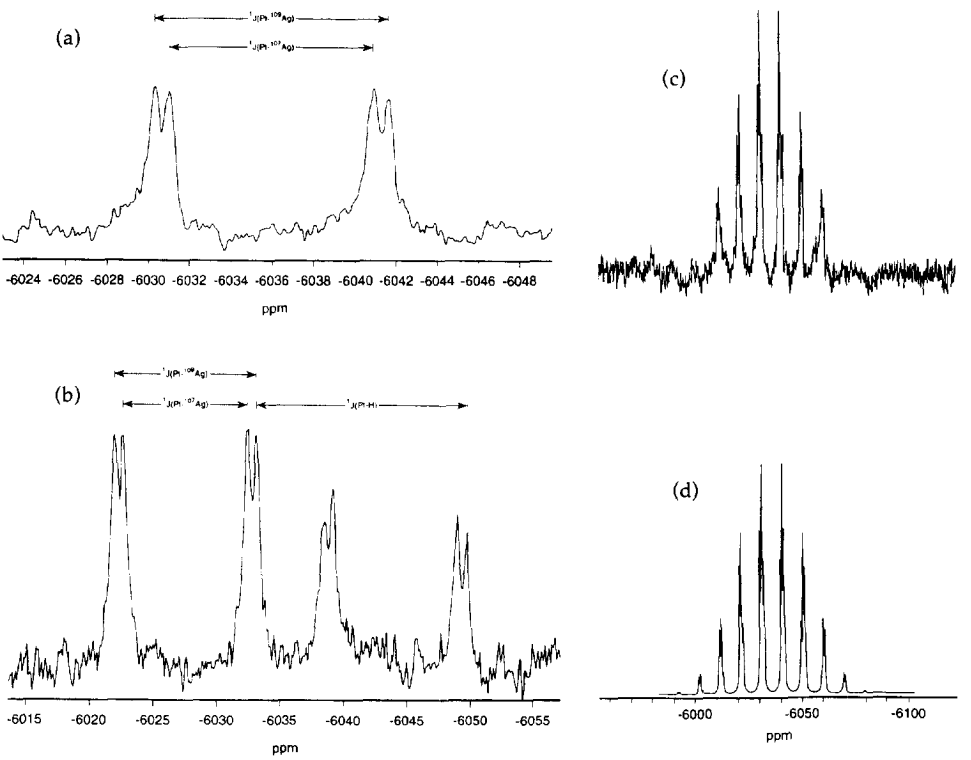

Fig. 13. ^{195}Pt NMR spectra of $[Pt(H)(Ag)(AuPPh_3)_8]^{2+}$ showing (a) the spectrum with both ^{31}P and ^1H decoupling, (b) with only ^{31}P decoupling, (c) with only ^1H decoupling, and (d) the simulated $^{195}Pt(^1H)$ spectrum shown in (c) using the coupling constants given in the text. The spectra were recorded at 43.02 MHz in CD_2Cl_2 solutions with K_2PtCl_6 in D_2O as external reference. Adapted from Ref. [34].

striking observation is that the cluster hydrido ligands have chemical shifts which are significantly shifted to the low field side of TMS ($\delta = 0.3$–5.4 ppm) compared with the normal upfield range for mononuclear (terminal) and binuclear (bridging) platinum hydrides (typically $\delta = -2$ to -9 ppm) [56]. These unusual shifts and the absence of terminal Pt—H stretching vibrations in the IR have been used to support a bridging bonding mode for the hydrido ligand [2,21,34]. The variable-temperature ^{1}H NMR spectra of $[Pt(AuPPh_3)_8]^{2+}$ under 1 atm of H_2 are shown in Fig. 14 [2]. The presence of bound, hydrido ligands in equilibrium with free H_2 is clearly evident by observation of the nonet pattern at 3.9 ppm with ^{195}Pt satellites at the lower temperatures. It is sometimes difficult to observe the ^{1}H NMR signal of Pt—Au cluster hydrides because of the low intensity of the multiplet signal and interference from ligand and solvent resonances. The use of ^{2}H NMR with cluster deuterides may be helpful in these cases.

^{13}C NMR of ^{13}C-enriched carbonyl-containing M—Au clusters has been used primarily as a method of characterization. Chemical shift and coupling constant data for some of the clusters are given in Table 4. In all known CO-containing M—Au clusters the CO ligand is bonded to the central metal in a terminal fashion. This has been determined by X-ray diffraction and IR data. The C—^{31}P coupling pattern is a good indicator of the number of PPh_3 groups bound to the Au and M atoms. As an example the ^{13}C NMR spectrum of $[Pt(^{13}CO)(PPh_3)(AuPPh_3)_5]^+$ is shown in Fig. 15 [17]. The chemical shifts δ of the CO carbon atoms are in the range 198–230 ppm (relative to external TMS) and are found substantially downfield from the chemical shifts in monomeric CO Pt complexes ($\delta = 149$–182 ppm) [57]. These chemical shifts are unusual and have not been explained. The $^1J(C—^{195}Pt)$ coupling constants show some general trends, but these are based on only a few examples. The +2 charged clusters have smaller $^1J(C—^{195}Pt)$ values than

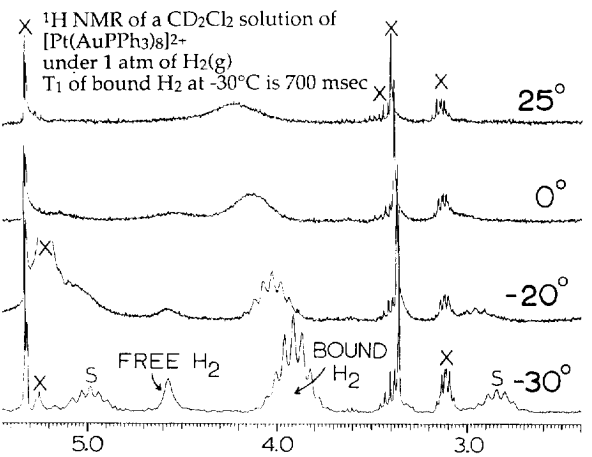

Fig. 14. ^{1}H NMR spectra of $[Pt(AuPPh_3)_8]^{2+}$ at different temperatures with use of CD_2Cl_2 as solvent at 1 atm H_2 pressure. The S symbols indicate ^{195}Pt satellites. Adapted from Ref. [3].

Table 4
^{13}C nuclear magnetic resonance and IR data for carbonyl M—Au cluster compounds

Compound	^{13}C NMR data[a]				ν(CO)[b] (cm^{-1})	Ref.
	δ (ppm)	J(C—Pt)	^2J(C—P)	^3J(C—P)		
$[Pt(CO)(PPh_3)_2(AuPPh_3)_3]^+$	198.3	1352	15.6	—	1974	[13]
$[Pt(CO)(PPh_3)(AuPPh_3)_5]^+$	208.4	1330	13.2	3.0	1946	[17]
$[Pt(CO)(PPh_3)(AuPPh_3)_6]^{2+}$	208.2	1200	14.2	4.2	1967	[17]
$[Pt(CO)(AuPPh_3)_8]^{2+}$	210.7	1256	11.0	—	1940	[15]
$[Pt(CO)(AgNO_3)(AuPPh_3)_8]^{2+}$	208.1	1226	10.0	—	1964	[14]
$[Pd(CO)(AuPPh_3)_8]^{2+}$	229.7	—	11.7	—	1955	[16]
$[Pd(CO)(AuCl)_3(AuPPh_3)_7]^+$	217.5	—	4.5	—	1979	[30]
$[Pd(CO)(AuBr)_3(AuPPh_3)_7]^+$	217.9	—	7.5	—	1977	[30]

[a] $CDCl_3$, ambient temperature, reference to TMS.
[b] KBr disk.

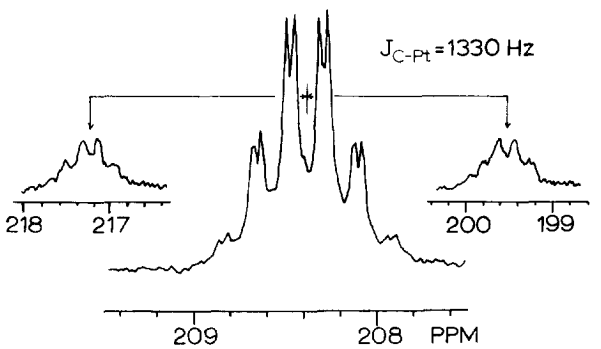

Fig. 15. ^{13}C NMR spectrum of $[Pt(^{13}CO)(PPh_3)(AuPPh_3)_5]^+$ in $CDCl_3$ solution at 25 °C. The ^{195}Pt satellite peaks are shown in the same vertical scale, but the horizontal scale has been compressed for clarity. Reproduced with permission from the American Chemical Society, Ref. [17].

those with +1 charges and the addition of an electrophile such as $AgNO_3$ to $[Pt(CO)(AuPPh_3)_8]^{2+}$ lowers the value of $^1J(C-^{195}Pt)$.

5.4. X-ray photoelectron spectroscopy

XPS spectra have been recorded for a large number of Pt—Au cluster compounds [50]. The Au $4f_{7/2}$ binding energies in all the cluster compounds studied are similar (range, 84.57–85.07 eV) and are shifted to higher values compared with Au(0) in metallic gold (84.20 eV), but are lower than Au(I) in $AuPPh_3NO_3$ and $AuPPh_3Cl$ (85.37 and 85.55 eV) and lie in the same range found for gold clusters examined previously [58]. The cluster compounds which contain π acceptor ligands such as CN, CO, or CNR on the Pt (average $E_b = 72.7$ eV) have higher Pt $4f_{7/2}$ E_b values than the other Pt-centered cluster compounds (average $E_b = 72.2$ eV). The effective

charge of the central Pt atom in these clusters varies over a wide range, and in some cases may not differ significantly from that of the peripheral Au atoms. The XPS data for the Hg $4f_{7/2}$ peak in the Hg-containing clusters show the effective charge on Hg to be between 1+ and 0. The XPS results are important in establishing the relative effective charges on the metal atoms in these clusters but otherwise do not add much information about the nature of these clusters.

6. Applications in catalysis

6.1. General

Many of the phosphine-stabilized, cationic M—Au cluster compounds discussed above have unusual reactivity and catalytic properties and offer some special opportunities for study. For example, (a) they show fast and clean H_2 activation catalysis under homogeneous and heterogeneous (gas–molecular solid) conditions (H_2-D_2 equilibration, hydrogenation of ethylene, hydrogenation of O_2, and D_2–H_2O exchange) [1–3], (b) they form hydrides in a variety of solvents that are stable in the presence of water, (c) the phosphine ligands provide a selective, hydrophobic, protective barrier around the cluster giving rise to narrow channels into the metal core as shown in the space filling drawings in Fig. 16, (d) they can be reversibly adsorbed onto silica and alumina solid supports where they are "intact" and exhibit similar reactivity to that of mulecular clusters in solution including H_2 activation catalysis and reaction with CO [59], and (e) they exhibit a wide variety of compositions that include changes of the central metal M (Pt, Pd, Ni, Au, Ru, Os, Ir, Rh,

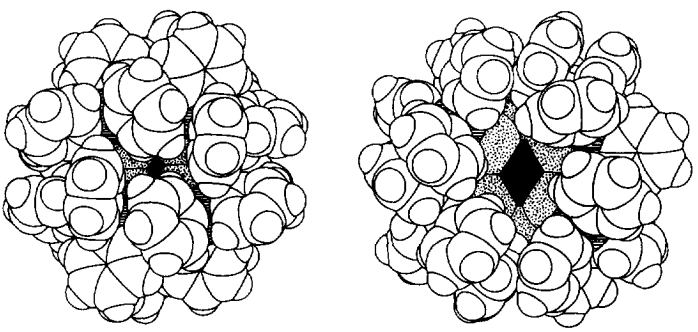

Fig. 16. Space filling drawings of the cluster dications $[Pt(AuPPh_3)_8]^{2+}$ and $[Pt(CO)(AuPPh_3)_8]^{2+}$ showing views with the largest openings to the Pt center. The CO ligand is removed from $[Pt(CO)(AuPPh_3)_8]^{2+}$ as this 18-electron cluster is a good model for $[Pt(H)_2(AuPPh_3)_8]^{2+}$. The Pt atoms are black, Au atoms speckled, and P atoms marked with horizontal, parallel lines. The approximate dimensions (smallest cross-section and depth) of the hydrophobic cavities are 1.5 Å × 4 Å and 8.5 Å and 5 Å × 6 Å and 7 Å respectively for $[Pt(AuPPh_3)_8]^{2+}$ and the CO adduct.

and Re), the third metal M′ (e.g. for $[PtM'_x(AuPPh_3)_y]^{n+}$ M′=Cu, Ag, Hg, and Sn), and the ligands (e.g. alkyl and aryl phosphines, halides, hydrides, isonitriles, and nitrate). These cluster compounds are being studied as models for polymetallic surface catalysts under homogeneous and heterogeneous conditions with the goals of determining structure–reactivity relations and understanding the surprising synergism known for transition metal–gold, –silver, and –copper catalysts [11]. Some of the clusters may also function as practical catalysts for H–D exchange between D_2 and H_2O (see below).

6.2. H_2–D_2 equilibration catalysis

Platinum– and palladium–gold cluster compounds (for example, $[Pt(AuPPh_3)_8](NO_3)_2$, Fig. 1) have recently been shown to be excellent catalysts for H_2–D_2 equilibration under homogeneous and heterogeneous (gas–molecular solid) conditions [1–3]. This equilibration reaction ($H_2+D_2 \rightleftharpoons 2HD$) has $K_{eq}=3.3$ at 30 °C and is commonly used as a quantitative measure of H_2 activation by surface catalysts [60]. Turnover rates for HD production with use of $[Pt(AuPPh_3)_8](NO_3)_2$ as the catalyst are 0.36 mol HD (mol cluster)$^{-1}$ s^{-1} and $\approx$5 mol HD (mol cluster)$^{-1}$ s^{-1} respectively for homogeneous (acetonitrile solution) and heterogeneous (gas–molecular solid) conditions (1 atm total pressure and 30 °C). These rates are among the fastest reported thus far for any molecular compound and the activity of the crystalline molecular solid is comparable with that of activated platinum surfaces [60,61]. The reaction is clean showing no H–D exchange with the PPh_3 ligands or solvents such as acetonitrile, nitrobenzene, dichloromethane, water, and ethanol. The first step of the mechanism of this catalysis reaction is thought to be the reversible addition of H_2 to $[Pt(AuPPh_3)_8]^{2+}$ as shown in Eq. (10) [3]. This equilibrium reaction has been directly observed by ^{31}P and ^{1}H NMR in solution and is rapidly reversible (see Figs. 14 and 17). The equilibrium constant for reaction (10) and the first-order rate constant for dissociation of H_2 from $[Pt(H)_2(AuPPh_3)_8]^{2+}$ have been determined by NMR lineshape analysis (nitrobenzene solution, 30 °C, 0.5 atm H_2) and are 1.7×10^3 l mol^{-1} and 4.5×10^2 s^{-1} respectively [3]. T_1 measurements for the coordinated hydrogen atoms in $[Pt(H)_2(AuPPh_3)_8]^{2+}$ show that this is a classical dihydride and not a side-bonded η^2-H_2 [2,3]. There is good indirect evidence that the hydride ligands are in bridging positions (see arguments presented above). Reaction (10) also takes place rapidly in the solid state and can be monitored by UV–visible spectroscopy (visible color change), and by H_2 uptake measurements. Approximately 0.9 mol of H_2 is bound to 1 mol of the cluster in the solid state at 1 atm and 25 °C [2].

Although the structure of the 18-electron cluster $[Pt(H)_2(AuPPh_3)_8]^{2+}$ has not been determined, it is likely to be spheroidal and UV–visible absorption data suggest it is similar to that of $[Pt(CO)(AuPPh_3)_8]^{2+}$. The space filling drawing of $[Pt(CO)(AuPPh_3)_8]^{2+}$ with the CO removed (Fig. 16) is therefore a reasonable representation for $[Pt(H)_2(AuPPh_3)_8]^{2+}$. Note that this compound has a much larger opening to the $PtAu_8$ core enabling access of larger substrates. This could be important in understanding catalysis mechanisms (see below).

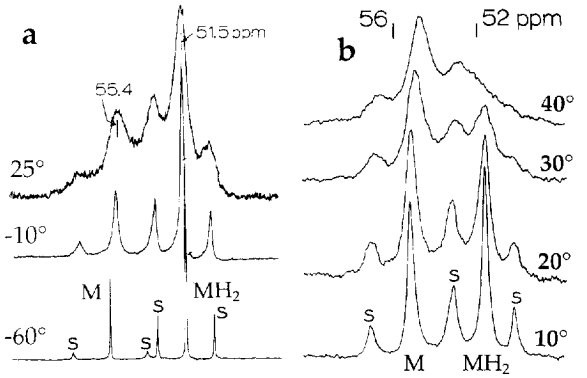

Fig. 17. $^{31}P(^{1}H)$ NMR spectra of $[Pt(AuPPh_3)_8](NO_3)_2 = M$ (3.6×10^{-3} M) at different temperatures with use of (a) CH_2Cl_2 as solvent at 1 atm H_2 pressure and (b) NO_2Ph as solvent at 0.5 atm H_2 pressure. The S symbols indicate ^{195}Pt satellites. Reproduced with permission from the American Chemical Society, Ref. [3].

6.2.1. *Rate data*

6.2.1.1. Homogeneous solution conditions. Rates for the catalytic production of HD from an equimolar mixture of H_2 and D_2 have been determined for a series of M—Au cluster compounds under homogeneous conditions [3]. A typical reaction profile is shown in Fig. 18 [3]. The formation of HD showed first-order kinetics and rates are reported as turnover frequencies with units of moles of HD per mole of cluster per second. Data for some of the clusters with use of nitrobenzene as solvent are reported in Table 5. Rates with use of acetonitrile are faster because of the higher solubility of H_2, but otherwise show the same general trends. The cluster compounds listed in the table are sorted by electron count (16 and 18) and by composition (hydrido and trimetallic) as this simplifies a discussion of the results. Rate data for several monometallic compounds are also listed for comparison. It is important to emphasize that the catalytic production of HD in nitrobenzene solution is a true homogeneous reaction and is not caused by solid impurities or irreversible cluster decomposition to colloidal metal. The rates are also not limited by gas–solution diffusion because they are first order in cluster concentration for the concentration range reported ($(2.5–6.4) \times 10^{-4}$ M). Numerous control experiments were carried out to demonstrate the homogeneous nature of this reaction [3].

Some general trends are apparent from the rate data shown in Table 5. 16-electron clusters have faster turnover rates than non-hydrido 18-electron clusters, but hydrido 18-electron clusters show rates that are similar to their 16-electron non-hydrido analogs. The effect on rate of the central metal in MAu_8 clusters is very pronounced with Pt ≫ Pd ≫ Au. 16-electron, platinum-centered clusters with the larger number of Au or Cu atoms generally have faster turnover rates as evidenced by the order $PtCuAu_8 > PtAu_8 > PtAu_6 > PtAu_0$ ($PtAu_3 > PtAu_6$ is the only exception). This trend is also followed with 18-electron, hydrido clusters where $[Pt(H)(PPh_3)(AuPPh_3)_7]^{2+}$

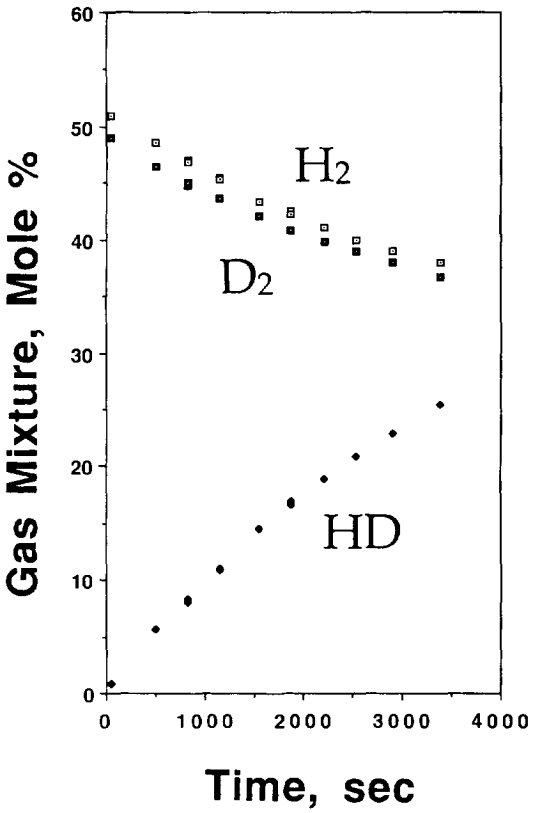

Fig. 18. Typical reaction profile for H_2–D_2 equilibration with the cluster catalyst $[Pt(AuPPh_3)_8]^{2+}$, 6.4×10^{-4} M in nitrobenzene solution, at 30 C and 1 atm. Reproduced with permission from the American Chemical Society, Ref. [3].

gave a faster turnover rate than $[Pt(H)(PPh_3)(AuPPh_3)_6]^+$. The very stable, 18-electron supracluster is inactive for H_2-D_2 equilibration. The trend of increasing rate with increasing Au : Pt ratio for 16-electron and 18-electron hydrido clusters has mechanistic implications (see below) and may be important for an understanding of H_2 activation on bimetallic surfaces that contain gold or copper. It is well documented that the hydrido ligands in M—Au clusters are bridging (see above). This rate trend therefore suggests that M—Au bonds in solid M—Au catalysts may serve as active sites for H_2 activation. The cluster $\{Pt[AuP(p\text{-}CH_3C_6H_4)_3]_8\}^{2+}$ showed a threefold increase in turnover rate compared with its triphenylphosphine analog. This shows that a more electron-rich cluster is more reactive for H_2 activation, in agreement with general observations from metal hydride chemistry. Finally, the 16-electron, coordinatively unsaturated compound $Pt(C_2H_4)(PPh_3)_2$ is more than an order of magnitude less active for H_2-D_2 equilibration than the 16-electron Pt—Au cluster compounds. This result supports the trend that the presence of Pt—Au bonds increases the activity of Pt catalysts. The above trends and implications have been

Table 5
Rate data for cataltyic H_2 D_2 equilibration under homogeneous conditions[a]

Compound	Turnover rate ($\times 10^2$ s^{-1}) for HD production
16-electron compounds	
$\{Pt[AuP(p\text{-tolyl})_3]_8\}(NO_3)_2$	22
$[Pt(AuPPh_3)_8](NO_3)_2$	7.5
$[Pt(PPh_3)(AuPPh_3)_6](NO_3)_2$	2.1
$[Pt(PPh_3)_2(AuPPh_3)_3]NO_3$	4.2
$[Pd(AuPPh_3)_8](NO_3)_2$	0.10
$[Au(AuPPh_3)_8](NO_3)_3$	0
$Pt(C_2H_4)(PPh_3)_2$	0.11
trans-$IrCl(CO)(PPh_3)_2$	0.15
18-electron compounds	
$[Pt(CO)(AuPPh_3)_8](NO_3)_2$	0.71
$[Pt(RNC)(AuPPh_3)_8](NO_3)_2$	0.20
$[Pt(PPh_3)(AuPPh_3)_7]NO_3$	0.16
$[Pt_3Au(\mu\text{-}CO)_3(PPh_3)_5]NO_3$	0.3
18-electron hydrido compounds	
$[Pt(H)(PPh_3)(AuPPh_3)_7](NO_3)_2$	7.7
$[Pt(H)(PPh_3)(AuPPh_3)_6]NO_3$	2.1
Trimetallic compounds	
$[Pt(CuCl)(AuPPh_3)_8](NO_3)_2$	15
$[Pt(AgNO_3)(AuPPh_3)_8](NO_3)_2$	4.0
$[Pt(H)(AgNO_3)(AuPPh_3)_8]NO_3$	4.4
$[Pt(HgNO_3)(PPh_3)(AuPPh_3)_6]NO_3$	0.60
$Pt_2Ag_{13}(AuPPh_3)_{10}Cl_7$	0

[a] Adapted from Ref. [3].

determined from the results of solution rate data. Since the H_2-D_2 equilibration reaction is complex mechanistically (two bonds must be broken and H—D scrambling must occur), some of these trends could result from differences in reaction mechanism for the various catalysts. For example, with the 18-electron hydrido clusters only one bond needs to break to produce HD.

6.2.1.2. Heterogeneous conditions. Several of the cluster compounds are also excellent catalysts for H_2-D_2 equilibration in the solid state (gas–molecular solid reaction) with turnover rates as high as $\approx 5\ s^{-1}$ and $2\ s^{-1}$ measured for powdered samples of $[Pt(AuPPh_3)_8](NO_3)_2$ and $[Pt(PPh_3)(AuPPh_3)_6](NO_3)_2$ respectively, at 1 atm pressure and 30 °C [3]. In the calculation of these turnover rates it was assumed that all cluster molecules are active sites. These rates are significantly greater than under homogeneous solution conditions and there is a marked dependence on surface area making meaningful comparisons between different samples difficult. The greatest rates were observed with finely divided powders. Control experiments showed that the catalysis was not caused by undetectable metallic Pt impurities [3]. It is surprising that these clusters are so active in the solid state where phosphine dissociation

or cluster fragmentation is unlikely. There have been only a few reports on molecular solid–gas catalytic transformations with organometallic compounds [62]. This general area is virtually unexplored and of obvious importance because of the high reactivity and different selectivity of some organometallic molecular solids [62].

6.2.2. Mechanism of the reaction

A large number of kinetic and control experiments were carried out in order to study the mechanism of the homogeneous, catalytic H_2-D_2 equilibration reaction [3]. The data clearly showed that the H_2-D_2 equilibration carried out in solution phase is a true homogeneous reaction and not the result of cluster fragmentation. In addition, mechanisms which lead to HD production do not involve heterolytic cleavage of H_2. There are two types of clusters that gave good reaction rates, 16-electron clusters exemplified by $[Pt(AuPPh_3)_8]^{2+}$, and 18-electron hydrido clusters exemplified by $[Pt(H)(PPh_3)(AuPPh_3)_7]^{2+}$. Since the former type of cluster does not contain hydride ligands, the production of HD must involve the addition of two molecules of reactant (H_2 and D_2) to the same cluster. With hydrido clusters, only one molecule of H_2 or D_2 is needed to produce HD. The mechanistic study was focused on these two prototype clusters with the mechanistically more demanding 16-electron $[Pt(AuPPh_3)_8]^{2+}$ receiving the most attention.

6.2.2.1. $[Pt(AuPPh_3)_8]^{2+}$. This cluster offers the best opportunity for a mechanistic study because the reversible addition of H_2 (Eq. (10)) has been directly observed (Figs. 14 and 17) and equilibrium constants and kinetic parameters have been determined experimentally by NMR [2,3] (see above). The results are consistent with a mechanism that involves the stepwise addition of two molecules of $(H,D)_2$ to the cluster M leading to a 20-electron, tetra(hydrido–deuterio) species $M(H,D)_4$. The notation $(H,D)_2$ represents the three isotope possibilities H_2, D_2, and HD. Such an intermediate or activated complex will rapidly scramble H and D and give HD via the reverse reactions. A similar mechanism has been proposed for catalytic H_2-D_2 equilibration by *trans*-$Ir(X)(CO)(PPh_3)_2$ (X=Cl, Br, I) [63] and can be represented by Eq. (46). In this equation, $M=[Pt(AuPPh_3)_8]^{2+}$.

$$M \underset{-(H,D)_2}{\overset{+(H,D)_2}{\rightleftharpoons}} M(H,D)_2 \underset{-(H,D)_2}{\overset{+(H,D)_2}{\rightleftharpoons}} M(H,D)_4 \tag{46}$$

It was shown from the NMR lineshape analysis results that the rate of the first step in Eq. (46), the addition of the first H_2 to $[Pt(AuPPh_3)_8]^{2+}$, is more than 10^3 times faster than the observed rate of HD production. This indicates that the formation of a tetra(hydrido–deuterio) species such as $M(H,D)_4$ is the rate-limiting step. This is reasonable because the formation of a 20-electron cluster is expected to be difficult. It follows from the above mechanism that the observed rate of HD production is given by [3]

$$\text{rate of HD production} = k_2[M(H,D)_2][(H,D)_2] \tag{47}$$

Eq. (47) requires that the rate of HD production is first order in $[M(H,D)_2]$ and

$[(H,D)_2]$. The kinetic data for variation of cluster concentration and partial pressure of $(H,D)_2$ were in agreement with this [3].

Although the mechanism shown by Eq. (46) for $[Pt(AuPPh_3)_8](NO_3)_2$ is reasonable and consistent with the rate data, the addition of several mole equivalents of PPh_3 inhibited the rate of HD production showing that an additional step was required [3]. However, interaction of added PPh_3 with M or MH_2 was not detected by $^{31}P(^1H)$ NMR or UV–visible spectroscopy. The most reasonable explanation for these observations is that a PPh_3 ligand reversibly dissociates from the dihydride cluster $[Pt(H)_2(AuPPh_3)_8]^{2+}$ to give an undetectable amount of a more reactive, coordinatively unsaturated species such as shown in [3]

$$[Pt(H)_2(AuPPh_3)_8]^{2+} \rightleftharpoons [Pt(H)_2(Au)(AuPPh_3)_7]^{2+} + PPh_3 \quad (48)$$

Although this equilibrium probably lies to the left, it could be difficult to observe the dissociation products by NMR and UV–visible spectroscopy [3]. The addition of excess PPh_3 would shift the equilibrium to the left by Le Chatelier's principle, thereby decreasing the amount of the catalytically active species. This mechanism helps to rationalize the formation of the 20-electron, tetrahydrido species from $[Pt(H)_2(AuPPh_3)_8]^{2+}$ by providing an open Au site to bind the incoming D_2. Formally, the replacement of a PPh_3 ligand on a Au atom with a η^2-D_2 ligand does not increase the electron count of the cluster core, thus avoiding the 20-electron count for this species. This type of mechanistic step is also common in homogeneous catalysis with organometallic compounds [64].

Catalytic studies with metal cluster compounds are always complicated by the possibility of cluster break-up or fragmentation. Such fragments have not been observed by spectroscopy and would have to be extremely active to give the observed rates. Possible candidates would be highly unsaturated small Pt—Au clusters. Such species would be very susceptable to poisoning by the addition of CO. The addition of 0.4 mole equivalents of CO slowed the rate of HD production only by 30%, consistent with formation of the inactive cluster $[Pt(CO)(AuPPh_3)_8]^{2+}$ [3]. This observation provides good evidence that cluster break-up is not the cause of catalytic HD production.

6.2.2.2. $[Pt(H)(PPh_3)(AuPPh_3)_7]^{2+}$. The 18-electron, hydrido clusters are also good catalysts for H_2-D_2 equilibration in solution and do not cause H—D exchange with the solvent, water, or alcohol. The presence of a hydride or deuteride ligand in the starting cluster provides an easier mechanism for HD production. The rate data for $[Pt(H)(PPh_3)(AuPPh_3)_7](NO_3)_2$ were consistent with a mechanism where the rate-limiting step is the addition of $(H,D)_2$ to give a 20-electron, $M(H,D)_3$ intermediate or activated complex [3]. Such an intermediate would rapidly scramble H and D and the reverse reaction would produce HD. In agreement with this, NMR results showed that $[Pt(H)(PPh_3)(AuPPh_3)_7]^{2+}$ was rapidly converted into $[Pt(D)(PPh_3)(AuPPh_3)_7]^{2+}$ under a D_2 atmosphere with nitrobenzene as solvent. PPh_3 inhibition experiments with $[Pt(H)(PPh_3)(AuPPh_3)_7]^{2+}$ showed similar results to those observed with $[Pt(AuPPh_3)_8]^{2+}$. Therefore, a reversible and spectro-

scopically unobservable dissociation of PPh_3 was implicated for activation, just as with $[Pt(AuPPh_3)_8]^{2+}$ [3].

6.2.2.3. Heterogeneous reaction. The fact that these clusters catalyze H_2-D_2 equilibration in the solid state at faster rates than in solution is surprising, especially since a phosphine dissociation step is implicated in solution. The faster rates observed with molecular solids probably result because there is no solvent present to compete with the second $(H,D)_2$ addition and diffusion into the porous crystals easily occurs. Crystals of these clusters are very porous and contain a significant amount of empty space because of the loss of solvent on removal from the crystallizing solution. Single-crystal X-ray analysis of these compounds require special crystal handling techniques such as sealed capillary tubes that contain some solvent. Even with this technique the solvent molecules, counteranions, and sometimes the ligand phenyl rings are disordered. It is possible that a PPh_3 ligand can partly dissociate in the solid, especially after solvent loss, thus producing an activated cluster. More work is needed to understand this heterogeneous, catalytic reaction. Current studies are aimed at measuring the effect of the ligand, counteranion, and crystallizing solvent.

6.2.3. Conclusions

Mixed Pt–Au cluster compounds have been shown to be excellent and clean catalysts for H_2-D_2 equilibration under homogeneous and heterogeneous conditions. These compounds therefore have the potential to serve as models for bimetallic surface catalysts. There is a significant rate effect on cluster size and metal composition. The most important effects are that (a) faster rates were observed as the Au:Pt ratio increased, (b) Pt-centered clusters gave faster rates than Pd-centered clusters, while Au clusters were inactive, and (c) 16-electron clusters gave much faster rates than 18-electron clusters, but 18-electron hydrido clusters were also fast. These trends suggest that M–Au bonds may function as the active sites for H_2 activation (M–Au cluster hydrides have bridging μ-H bonding modes) with Pt–Au bonds being more effective than Pd–Au bonds. This result helps explain how Au can increase the activity of Pt–Au surfaces and suggests that Au plays a direct role in H_2 activation. These suggestions are complicated, however, by the fact that PPh_3 dissociation is necessary for catalyst activation. An open Au site may be necessary for binding the second $(H,D)_2$ so that H–D exchange can take place on the cluster. Weak binding of substrates by Au in Pt–Au surface catalysts has been observed [11].

6.3. D_2–H_2O isotope exchange catalysis

A new and potentially useful, homogeneous, catalytic reaction with several Pt–Au cluster compounds has recently been reported [65]. In pyridine solution, the cluster $[Pt(AuPPh_3)_8]^{2+}$ showed surprisingly fast exchange between D_2(gas) and H_2O(liquid). Thus, reaction of D_2 with a pyridine solution of the cluster that contained some H_2O gave fast production of H_2 and HD (turnover rate, 1.5 min^{-1} at 1 atm total pressure and 30 °C; Table 6). A typical reaction profile is shown in Fig. 19. Data for the control reaction carried out with wet nitrobenzene (saturated

Table 6
Rate of D_2-ROH and D_2 H_2O exchange reactions for various catalysts under homogeneous conditions [65]

Catalyst	Reactants	Observed product	Turnover rate (min^{-1})	Solvent-promoter	Ref.
$Ru(OEP)(THF)(\eta^2\text{-}H_2)$[a]	H_2+D_2O (0.1 M)[b]	HD, D_2	0.02	THF−KOD (0.1 M)	[66a]
$W(CO)_3(P\text{-}i\text{-}Pr_3)_2(\eta^2\text{-}D_2)$	D_2+H_2O (0.04 M)[c]	HD, H_2	ca. 1×10^{-4}	THF−none	[66b]
$[Pt(AuPPh_3)_8]^{2+}$	D_2+H_2O (0.1 M)[c]	HD, H_2	1.5[d]	Pyridine−none	[65]
$RhCl(PPh_3)_3$	D_2+t-BuOH (1 M)[c]	t-BuOD	0	CH_2Cl_2 −none	[66c]
$[CpRu(CO)(PPh_3)(\eta^2\text{-}H_2)]^+$	D_2+t-BuOH (1 M)[c]	t-BuOD	0.1	CH_2Cl_2−none	[66c]
$[Ru(dppe)_2(H)(\eta^2\text{-}H_2)]^+$	D_2+t-BuOH (1 M)[c]	t-BuOD	2	CH_2Cl_2−none	[66c]
$[Ir(bq)(PPh_3)_2H(\eta^2\text{-}H_2)]^+$[e]	D_2+t-BuOH (1 M)[c]	t-BuOD	27	CH_2Cl_2−none	[66c]
$[Ni(SNO)_2]^{2+}$[f]	D_2+EtOH (2 M)[c]	EtOD	2	DMSO HBF_4	[66d]
$Rh(H)(CO)(^{bu}S_4)$[g]	D_2+EtOH (0.8 M)[h]	EtOD	5×10^{-3}	THF−HCl (0.04 M)	[66e]
$H_2PtCl_6-SnCl_2$[i]	D_2+MeOH (neat)[j]	HD, H_2	ca. 7×10^{-3}	MeOH−none	[66f]

[a] OEP, octaethylporphyrin.
[b] $P(H_2)=0.1$ atm, 50 °C.
[c] 1 atm pressure and ambient temperature.
[d] Rate determined for decrease in D_2 concentration for the first hour of reaction where the change in concentration with time is linear.
[e] bq, 7,8-benzoquinolinato.
[f] SNO, $o\text{-}C_6H_4(OH)=N-NHCSNH_2$.
[g] $^{bu}S_4$=((2-mercapto-3,5-di-*tert*-butylphenyl)thio)ethanato.
[h] 10 atm pressure.
[i] Mixture prepared in situ, rate reported for optimum Sn:Pt ratio.
[j] $P(D_2)=25$ Torr, 20 °C.

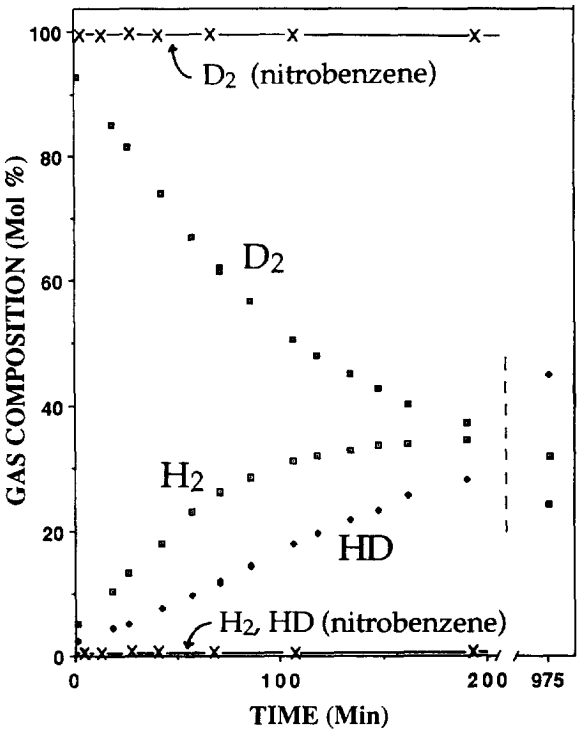

Fig. 19. Composition of the head space gas in mole per cent D_2, HD, and H_2 as a function of time for reaction of D_2 (1.3 mmol) with H_2O (0.6 mmol) in the presence of $[Pt(AuPPh_3)_8](NO_3)_2$ (4.0×10^{-6} mmol) in pyridine and nitrobenzene (– × –) solutions. The reactions were carried out in a closed, 38 ml reactor with 6 ml of rapidly stirred solution maintained at 1 atm total pressure and 30 °C. The points at the far right (975 min) are the mole per cents for the reaction in pyridine close to equilibrium. Reproduced with permission from the American Chemical Society, Ref. [65].

with H_2O) as solvent, where $(D_2)_g$–$(H_2O)_l$ exchange did not occur, are included in Fig. 19. Exchange was also not observed between $(D_2)_g$ and $(H_2O)_l$ with the (1:4 by volume) solvent mixtures H_2O:acetone or H_2O:methanol, run under the same conditions. Detailed reaction conditions are given in the figure caption. The exchange occurred with water and not with the pyridine solvent. Although $(D_2)_g$–$(H^+)_l$ exchange is known for a number of organometallic hydrides [66] (notably of the η^2-H_2 variety) and for hydrogenase enzymes [67], there are several factors which make this cluster-based system unusual. The exchange occurs between D_2 and water whereas with many metal complex based systems the exchange has only been reported between D_2 and alcohols (typically *t*-BuOH, EtOH or MeOH). For exchange with water, the rate is at least two orders of magnitude faster with $[Pt(AuPPh_3)_8]^{2+}$ than with monometallic complexes, although some faster rates have been observed with alcohols (see Table 6). $[Pt(AuPPh_3)_8]^{2+}$ is stable under the catalytic conditions and can carry out thousands of turnovers, while many organometallic hydrides are not stable in the presence of water. There is a need to develop stable catalysts for the

isotopic exchange between hydrogen and liquid water. Important applications include the production of heavy water and the removal of tritium from contaminated water [68].

Some of the key cluster intermediates in the catalytic exchange reaction have been observed by NMR spectroscopy. A $^{31}P(^{1}H)$ NMR study of $[Pt(AuPPh_3)_8]^{2+}$ in pyridine solution with various partial pressures of H_2 was undertaken. Reaction with ca. 0.1 atm of H_2 in a sealed NMR tube resulted in an equilibrium mixture of $[Pt(AuPPh_3)_8]^{2+}$, $[Pt(H)_2(AuPPh_3)_8]^{2+}$, and the monohydrido cluster compound $[Pt(H)(AuPPh_3)_8]^{+}$ as shown in Fig. 20 [65]. The cluster compound $[Pt(H)(AuPPh_3)_8]^{+}$ is not formed by the reaction of H_2 with $[Pt(AuPPh_3)_8]^{2+}$ in less basic solvents (e.g. nitrobenzene, dicholormethane, acetone, or acetonitrile) where only $[Pt(H)_2(AuPPh_3)_8]^{2+}$ is observed [2,3]. The formation of these hydrido clusters was rapid and reversible. Removal of the H_2 by a N_2 purge resulted in the fast, and quantitative reformation of $[Pt(AuPPh_3)_8]^{2+}$. These observations indicated that $[Pt(H)_2(AuPPh_3)_8]^{2+}$ was reversibly deprotonated by pyridine giving the monohydrido cluster $[Pt(H)(AuPPh_3)_8]^{+}$:

$$[Pt(H)_2(AuPPh_3)_8]^{2+} + Py \rightleftharpoons [Pt(H)(AuPPh_3)_8]^{+} + HPy^{+} \quad (49)$$

It was shown by NMR and UV–visible spectroscopy that $[Pt(AuPPh_3)_8]^{2+}$ does not form an observable adduct with pyridine in the absence of H_2. Recall, however, that $[Pt(H)_2(AuPPh_3)_8]^{2+}$ is likely to have a much larger access cavity into the metal core as shown in Fig. 16. This would permit the pyridine molecule to approach closely the bound hydrido ligands.

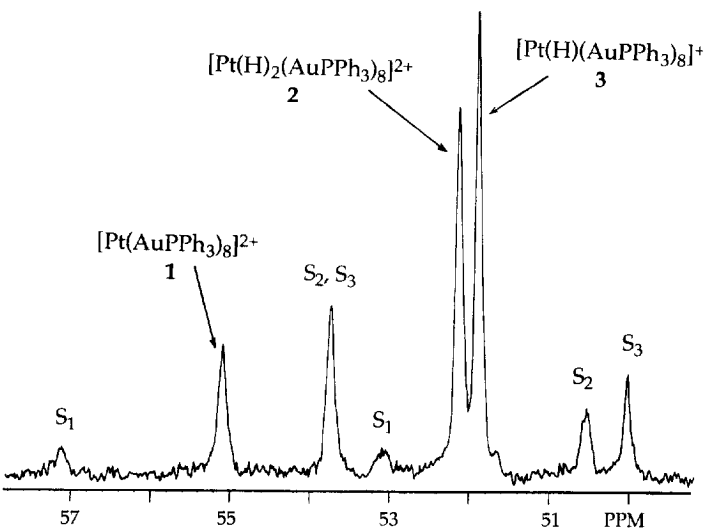

Fig. 20. $^{31}P(^{1}H)$ NMR spectrum of $[Pt(AuPPh_3)_8](NO_3)_2$ (3×10^{-3} M) in pyridine solution at ambient temperature under ca. 0.1 atm of H_2. The compounds were identified by their chemical shifts and coupling constants. The peaks assigned as S_1 are the ^{195}Pt satellite resonances of compound **1** etc. Reproduced with permission from the American Chemical Society, Ref. [65].

A reasonable mechanism for the $(D_2)_g$–$(H_2O)_l$ exchange reaction with $[Pt(AuPPh_3)_8]^{2+} = M^{2+}$ as the catalyst involves the following steps [65]:

$$M^{2+} + D_2 \rightleftharpoons M(D)_2^{2+} \quad \text{(slow)} \tag{50a}$$

$$M(D)_2^{2+} + Py \rightleftharpoons MD^+ + DPy^+ \tag{50b}$$

$$DPy^- + H_2O \rightleftharpoons HPy^+ + HDO \tag{50c}$$

$$HPy^+ + MD^+ \rightleftharpoons M(H)(D)^{2+} + Py \tag{50d}$$

$$M(H)(D)^{2+} \rightleftharpoons HD + M^{2+} \quad \text{(slow)} \tag{50e}$$

etc.

Only steps (50a)–(50c) are needed to achieve isotope exchange if one permits the H and D to be interchanged in the formulae and ignores kinetic isotope effects. The production of H_2 would result from $M(H)_2^{2+}$ which is formed by further exchange of $M(H)(D)^{2+}$ with H_2O by steps such as reactions (50b)–(50d). The gas composition with time plot for the reaction of D_2 with H_2O (Fig. 19) shows that H_2 is initially formed at a faster rate than HD, even though at equilibrium the concentration of HD is greater than that of H_2. This observation indicates that steps (50b) and (50c) occur at faster rates than step (50a). Thus the isotopic composition of the dihydrido species $M(H,D)_2^{2+}$ will be close to the composition in the liquid $(H,D)_2O$ phase, producing gas species of the same isotopic composition via the slower step (50a). The notation $(H,D)_2O$ refers to the three isotopic possibilites H_2O, HDO, and D_2O. In the reaction shown in Fig. 19, the initial liquid phase is H_2O giving $M(H)_2^{2+}$ as the major species. This results in H_2 as the major initial gas phase product as observed. The rate of HD formation will increase relative to that of H_2 as the amount of D increases in the liquid water phase, and so on to equilibrium. The final equilibrium distribution of D between the liquid and gas phases will be dictated by the equilibrium constants of the reactions between the liquid $(H,D)_2O$ and gaseous $(H,D)_2$ species [65]. More work is needed to test this mechanism and to determine the thermodynamics and kinetics of this interesting reaction.

A surprising property of these clusters is the rapid, reversible exchange of H_2 with the dihydride complex $[Pt(H)_2(AuPPh_3)_8]^{2+}$ (Eqn. (10), Figs. 14 and 17). This fast exchange is very unusual for a compound in which the hydrogen ligands are bound as classical hydrides. Such fast exchange usually implies η^2-H_2 bonding [66,69]; however, little is known about the exchange properties of cluster-bound, bridging hydrides. Indeed, Eq. (10) is the only known example of a simple (without ligand loss), reversible reaction between H_2 and a metal cluster compound [70].

7. Prospects for future studies

A large variety of M—Au cluster compounds have now been prepared and the synthetic methods have been sufficiently developed to permit planned syntheses of new target molecules. The field of cluster synthesis will continue to develop leading

to compounds with different stabilizing ligands, different metal combination and site preferences, and new giant clusters. It can be predicted that M—Au clusters which contain three, four, and more vertex-shared icosahedra as well as approximate M—Au analogs of clusters such as $[Au_{39}(PPh_3)_{14}Cl_6]Cl_2$ [71], $Au_{55}(PPh_3)_{12}Cl_6$ [72], and $[Pd_{561}Phen_{60}O_{60}][PF_6]_{60}$ [73] will be prepared. The primary difficulty in this field is cluster characterization. X-ray crystallography, NMR, and FABMS have been used extensively for the characterization of smaller clusters (up to 25 metal atoms) but these techniques are less useful with larger clusters. For example, it has been exceedingly difficult to grow X-ray quality, single crystals of larger clusters and, even with the use of a rotating anode X-ray source, many larger clusters cannot be structurally characterized. There is a need to apply different methods of characterization for larger clusters.

MS has great potential in cluster characterization. Techniques such as laser desorption–Fourier transform MS, electrospray, and ^{252}Cf plasma desorption MS are currently being used with some success [74,75]. Other techniques such as high resolution electron microscopy, transmission electron microscopy (TEM), scanning TEM, scanning tunneling microscopy, extended X-ray adsorption fine structure, and low angle X-ray scattering have been applied to the characterization of larger clusters and colloids [10], but these methods are difficult to use successfully. Applications of microscopy methods will surely continue and expand, especially as larger clusters are prepared. We are fast approaching the point where cluster chemistry is merging with the fields of colloid, materials, and surface chemistry [10,74]. This will provide great new challenges for the cluster chemist.

Another challenge in this field is to examine more fully the reactivity properties of metal cluster compounds. Many fascinating mixed-metal clusters have been prepared and characterized but there have been only a few thorough reactivity studies. It is very important to carry out careful kinetic and thermodynamic studies of fundamental reactions with metal clusters. This area is difficult because of problems with complex spectroscopic analysis, cluster rearrangements, and the possibility of cluster fragmentation. This is especially true for catalytic reactions. However, it is necessary to meet this challenge if the field of cluster chemistry is to have continued impact. The study of H_2 activation catalysis with M—Au clusters presented above provides a good example of the difficulty and usefulness of this approach. It is especially important for the cluster chemist to explore further the cluster–surface analogy. There is a great potential to advance significantly our understanding of bimetallic surface catalysis by studying reactions of bimetallic clusters.

Finally, cluster compounds have the potential to function as useful catalysts or catalyst precursors. There have been many catalytic studies with metal clusters, supported clusters, and supported, calcined (heated–decomposed) clusters [10]. Nearly all of these studies have utilized clusters stabilized primarily with CO ligands. Although these investigations have helped in our understanding of how surface catalysts function, very few have led to useful, practical catalysts. The use of metal cluster compounds as practical catalysts remains an unachieved goal. Work in this area should continue, especially with polymetallic clusters stabilized with ligands other than CO. This area remains an important challenge to the cluster chemist.

References

[1] M.A. Aubart and L.H. Pignolet, J. Am. Chem. Soc., 114 (1992) 7901.

[2] T.G.M.M. Kappen, J.J. Bour, P.P.J. Schlebos, A.M. Roelofsen, J.G.M. van der Linden, J.J. Steggerda, M.A. Aubart, D.A. Krogstad, M.F.J. Schoondergang and L.H. Pignolet, Inorg. Chem., 32 (1993) 1074.

[3] M.A. Aubart, B.D. Chandler, R.A.T. Gould, D.A. Krogstad, M.F.J. Schoondergang and L.H. Pignolet, Inorg. Chem., 33 (1994) 3724.

[4] P. Braunstein and J. Rose, in I. Bernal (ed.), Stereochemistry of Organometallic and Inorganic Compounds, Vol. 3, Elsevier, Amsterdam, 1988, p. 3.
P. Braunstein, in A.F. Williams, C. Floriani and A.E. Merbach (eds.), Perspectives in Coordination Chemistry, Helvetica Chimica Acta, Basle, 1992, p. 67.

[5] K.P. Hall and D.M.P. Mingos, Prog. Inorg. Chem., 32 (1984) 237.

[6] D.M.P. Mingos and M.J. Watson, Adv. Inorg. Chem., 39 (1992) 327.

[7] A.M. Mueting, W. Bos, B.D. Alexander, P.D. Boyle, J.A. Casalnuovo, S. Balaban, L.N. Ito, S.M. Johnson and L.H. Pignolet, New J. Chem., 12 (1988) 505.

[8] I.D. Salter, Adv. Organomet. Chem., 29 (1989) 249.

[9] J.J. Steggerda, Comments Inorg. Chem., 11 (1991) 113.

[10] B.C. Gates, L. Guczi and H. Knözinger, Metal Clusters in Catalysis, Elsevier, Amsterdam, 1986.
L.N. Lewis, Chem. Rev., 93 (1993) 2693.
D.M.P. Mingos, J. Cluster Sci., 3 (1992) 397.
G. Süss-Fink and G. Meister, Adv. Organomet. Chem., 35 (1993) 41.

[11] J. Schwank, K. Balakrishnan and A. Sachdev, in L. Guczi, F. Solymosi and P. Tetenyi (eds.), New Frontiers in Catalysis, Elsevier, Amsterdam, 1993, p. 905.
D. Rouabah and J. Friassard, J. Catal., 144 (1993) 30.
K. Balakrishnan and J. Schwank, J. Catal., 132 (1991) 451.
A. Sachdev and J. Schwank, J. Catal., 120 (1989) 353.
P.A. Sermon, J.M. Thomas, K. Keryou and G.R. Millward, Angew. Chem., Int. Edn. Engl., 26 (1987) 918.
K. Balakrishnan, A. Sachdev and J. Schwank, J. Catal., 121 (1990) 441.
R.C. Yeates and G.A. Somorjai, J. Catal., 103 (1987) 208.
J.H. Sinfelt, Bimetallic Catalysts, Wiley, New York, 1983.
J.K.A. Clarke, I. Manniger and T. Baird, J. Catal., 54 (1978) 230.

[12] D.M.P. Mingos and D.J. Wales, Introduction to Cluster Chemistry, Prentice-Hall, Englewood Cliffs, NJ, 1990.
D.M.P. Mingos and R.L. Johnson, Struct. Bonding, 68 (1987) 29.
A.J. Stone, Inorg. Chem., 20 (1981) 563.

[13] L.N. Ito, A.M.P. Felicissimo and L.H. Pignolet, Inorg. Chem., 30 (1991) 387.

[14] R.P.F. Kanters, P.P.J. Schlebos, J.J. Bour, W.P. Bosman, J.M.M. Smits, P.T. Beurskens and J.J. Steggerda, Inorg. Chem., 29 (1990) 324.

[15] R.P.F. Kanters, P.P.J. Schlebos, J.J. Bour, W.P. Bosman, H.J. Behm and J.J. Steggerda, Inorg. Chem., 27 (1988) 4034.

[16] L.N. Ito, A.M.P. Felicissimo and L.H. Pignolet, Inorg. Chem., 30 (1991) 988.

[17] L.N. Ito, J.D. Sweet, A.M. Mueting, L.H. Pignolet, M.F.J. Schoondergang and J.J. Steggerda, Inorg. Chem., 28 (1989) 3696.

[18] P.D. Boyle, B.J. Johnson, B.D. Alexander, J.A. Casalnuovo, P.R. Gannon, S.M. Johnson, E.A. Larka, A.M. Mueting and L.H. Pignolet, Inorg. Chem., 26 (1987) 1346.

[19] (a) A.J. Layton, R.S. Nyholm, G.A. Pneumaticakis and M.L. Tobe, Chem. Ind., 15 (1967) 465.
(b) P. Braunstein, H. Lehner, D. Matt, A. Tiripicchio and M. Tiripicchio-Camellini, Angew. Chem., Int. Edn. Engl., 23 (1984) 304.

[20] L.N. Ito, B.J. Johnson, A.M. Mueting and L.H. Pignolet, Inorg. Chem., 28 (1989) 2026.

[21] R.P.F. Kanters, J.J. Bour, P.P.J. Schlebos, W.P. Bosman, H.J. Behm, J.J. Steggerda, L.N. Ito and L.H. Pignolet, Inorg. Chem., 28 (1989) 2591.

[22] F. Cariati and L. Naldini, J. Chem. Soc., Dalton Trans., (1972) 2286.
[23] J.W. Lauher and K. Wald, J. Am. Chem. Soc., 103 (1981) 7648.
[24] D.G. Evans and D.M.P. Mingos, J. Organomet. Chem., 232 (1982) 171.
[25] D.A. Krogstad and L.H. Pignolet, to be submitted for publication.
[26] M.F.J. Schoondergang, J.J. Bour, G.P.F. van Strijdonck, P.P.J. Schlebos, W.P. Bosman, J.M.M. Smits, P.T. Beurskens and J.J. Steggerda, Inorg. Chem., 30 (1991) 2048.
[27] J.J. Bour, P.P.J. Schlebos, R.P.F. Kanters, M.F.J. Schoondergang, H. Addens, A. Overweg and J.J. Steggerda, Inorg. Chim. Acta, 181 (1991) 195.
[28] R.A.T. Gould and L.H. Pignolet, Inorg. Chem., 33 (1994) 40.
[29] R.A.T. Gould, J.S. Wiley, K.L. Craighead and L.H. Pignolet, submitted to Inorg. Chem.
[30] K.L. Craighead, A.M.P. Felicissimo, D.A. Krogstad, L.T.J. Nelson and L.H. Pignolet, Inorg. Chim. Acta, 212 (1993) 31.
[31] J.J. Bour, P.P.J. Schlebos, R.P.F. Kanters, W.P. Bosman, J.M.M. Smits, P.T. Beurskens and J.J. Steggerda, Inorg. Chim. Acta, 171 (1990) 177.
[32] J.J. Bour, W. van der Berg, P.P.J. Schlebos, R.P.F. Kanters, M.F.J. Schoondergang, W.P. Bosman, J.M.M. Smits, P.T. Beurskens, J.J. Steggerda and P. van der Sluis, Inorg. Chem., 29 (1990) 2971.
[33] M.F.J. Schoondergang, J.J. Bour, P.P.J. Schlebos, A.W.P. Vermeer, W.P. Bosman, J.M.M. Smits, P.T. Beurskens and J.J. Steggerda, Inorg. Chem., 30 (1991) 4704.
[34] T.G.M.M. Kappen, Ph.D. Thesis (ISBN 90 373 0252 1), University of Nijmegen, 1994.
[35] J.G.M. van der Linden, A.M. Roelofsen and G.H.W. Ipskamp, Inorg. Chem., 28 (1989) 967.
J.G.M. van der Linden, M.L.H. Paulussen and J.E.J. Schmitz, J. Am. Chem. Soc., 105 (1983) 1903.
[36] B.K. Teo and K. Keating, J. Am. Chem. Soc., 106 (1984) 2224.
B.K. Teo, M.C. Hong, H. Zhang and D.B. Huang, Angew. Chem., Int. Edn., Engl., 26 (1987) 897.
K. Teo and H. Zhang, Angew. Chem., Int. Edn. Engl., 31 (1992) 445.
[37] B.K. Teo, H. Zhang and X. Shi, J. Am. Chem. Soc., 112 (1990) 8552.
[38] B.K. Teo, X. Shi and H. Zhang, cited in Chem. Eng. News, 67 (1989) 6.
[39] B.K. Teo, H. Zhang and X. Shi, Inorg. Chem., 29 (1990) 2083.
[40] B.K. Teo, H. Zhang and X. Shi, J. Am. Chem. Soc., 115 (1993) 8489.
[41] T.G.M.M. Kappen, P.P.J. Schlebos, J.J. Bour, W.P. Bosman, J.M.M. Smits, P.T. Beurskens and J.J. Steggerda, Inorg. Chem., 33 (1994) 754.
[42] B.K. Teo, H. Zhang and X. Shi, Inorg. Chem., 33 (1994) 4086.
[43] D.M.P. Mingos and L. Zhenyang, Comments Inorg. Chem., 9 (1989) 95.
[44] E.W. Smith, A.J. Welch, I. Treurnicht and R.J. Puddephatt, Inorg. Chem., 25 (1986) 4616.
[45] A.G. Orpen, J. Chem. Soc., Dalton. Trans., (1980) 2509.
[46] B.D. Alexander, B.J. Johnson, S.M. Johnson, S.M. Johnson, A.L. Casalnouvo and L.H. Pignolet, J. Am. Chem. Soc., 108 (1986) 4409.
[47] C. Bianchini, A. Meli, M. Peruzzini, A. Vacca, F. Vizza and A. Albinati, Inorg. Chem., 31 (1992) 3841.
[48] B.K. Teo and H. Zhang, Polyhedron, 9 (1990) 1985.
[49] B.K. Teo, Coord. Chem. Rev., article in this volume.
[50] Y.M. Shul'ga, A.V. Bulatov, R.A.T. Gould, W.V. Konze and L.H. Pignolet, Inorg. Chem., 31 (1992) 4704.
[51] A. Mohtaser and R.W. Golightly, Inductively Coupled Plasma in Analytical Atomic Spectrometry, VCH, 1987.
[52] M.F.J. Schoondergang, Ph.D. Thesis (ISBN 90-9004964-9), University of Nijmegen, 1992.
[53] A. Albinati, F. Demartin, P. Janser, L.F. Rhodes and L.M. Venanzi, J. Am. Chem. Soc., 111 (1989) 2115.
[54] J.J. Bour, Ph.D. Thesis (ISBN 90-9003337-8), University of Nijmegen, 1992.
[55] R.P.F. Kanters, Ph.D. Thesis (ISBN 90-9003290-8), University of Nijmegen, 1992.
[56] D.P. Arnold and M.A. Bennett, Inorg. Chem., 23 (1984) 2110.
F. Bachechi, G. Bracher, D.M. Grove, B. Kellenberger, P.S. Pregosin, L.M. Venanzi and L. Zambonelli, Inorg. Chem., 22 (1983) 1031.
[57] B.E. Mann and B.F. Taylor, in P.M. Maitlis, F.G.A. Stone and R. West (eds.), Organometallic Chemistry, Academic Press, London, 1981, p. 181.
B.E. Mann, in J. Mason (ed.), Multinuclear NMR, Plenum, New York, 1987, Chap. 10.

[58] C. Battistoni, G. Mattogno and D.M.P. Mingos, J. Electron Spectrosc. Relat. Phenom., 33 (1984) 107. P.M.Th.M. van Attekum, J.W.A. van der Velden and J.M. Trooster, Inorg. Chem., 19 (1980) 701.
[59] I.V.G. Graf, J.W. Bacon, M.E. Curley, L.N. Ito and L.H. Pignolet, submitted to Inorg. Chem.
[60] G.C. Bond, Catalysis by Metals, Academic Press, New York, 1962, Chap. 8.
[61] H-W. Jen and A. Brenner, in Y. Yermakov and V. Likholobov (eds.), Proc. Vth Int. Symp. on Relations between Homogeneous and Heterogeneous Catalysis, Novosibirsk, USSR, 1986, p. 865.
[62] C. Bianchini, P. Frediani, M. Graziani, J. Kaspar, A. Meli, M. Peruzzini and F. Vizza, Organometallics, 12 (1993) 2886.
C. Bianchini, E. Farnetti, M. Graziani, J. Kaspar and F. Vizza, J. Am. Chem. Soc., 115 (1993) 1753.
A.R. Siedle and R.A. Newmark, Organometallics, 8 (1989) 1442.
[63] M.E. Tadros and L. Vaska, J. Colloid Interface Sci., 85 (1982) 389.
[64] C.A. Tolman and J.W. Faller, in L.H. Pignolet (ed.), Homogeneous Catalysis with Metal Phosphine Complexes, Plenum, New York, 1983, Ch. 2.
[65] M.A. Aubart, J.F.D. Koch and L.H. Pignolet, Inorg. Chem., 33 (1994) 3852.
[66] (a) J.P. Collman, P.S. Wagenknecht, J.E. Hutchison, N.S. Lewis, M.A. Lopez, R. Guilard, M. L'Her, A.A. Bothner-By and P.K. Mishra, J. Am. Chem. Soc., 114 (1992) 5654.
(b) G.J. Kubas, C.J. Burns, G.R.K. Khalsa, L.S. van der Sluys, G. Kiss and C.D. Hoff, Organometallics, 11 (1992) 3390.
(c) A.C. Albeniz, D.M. Heinekey and R.H. Crabtree, Inorg. Chem., 30 (1991) 3632.
(d) M. Zimmer, G. Schulte, X.-L. Lou and R.H. Crabtree, Angew. Chem., Int. Edn. Engl., 30 (1991) 193.
(e) D. Sellmann, J. Käppler and M. Moll, J. Am. Chem. Soc., 115 (1993) 1830.
(f) K. Hirabayashi and I. Yasumori, J. Chem. Soc., Faraday Trans. I, 69 (1973) 595.
(g) R.T. Hembre and S. McQueen, J. Am. Chem. Soc., 116 (1994) 2141.
[67] (a) J.A. Kovacs, in G.L. Eichhorn and L.G. Marzilli (eds.), Advances in Inorganic Biochemistry, Vol. 9, Prentice-Hall, Englewood Cliffs, NJ, 1993, Chap. 5, and references cited therein.
(b) R.H. Holm, in A.W. Addison, W.R. Cullen, D. Dolphin and B.R. James (eds.), Biological Aspects of Inorganic Chemistry, Wiley, New York, 1977, p. 71.
(c) S. Alvarez and R. Hoffmann, An. Quim., Ser. B, 82 (1986) 52.
(d) M. Teixeira, G. Fauque, I. Moura, P.A. Lespinat, Y. Berlier, B. Prickril, H.D. Peck, Jr., A.V. Xavier, J. Le Gall and J.J.G. Moura, Eur. J. Biochem., 167 (1987) 47.
[68] H.K. Rae, in H.K. Rae (ed.), Separation of Hydrogen Isotopes, ACS Symposium Series 68, American Chemical Society, Washington, DC, 1978, p. 1.
J.P. Butler, J.H. Rolston and W.H. Stevens, in H.K. Rae (ed.), Separation of Hydrogen Isotopes, ACS Symposium Series 68, American Chemical Society, Washington, DC, 1978, p. 93.
M.L. Rogers, P.H. Lamberger, R.E. Ellis and T.K. Mills, in H.K. Rae (ed.), Separation of Hydrogen Isotopes, ACS Symposium Series 68, American Chemical Society, Washington, DC, 1978, p. 171.
[69] M.S. Chinn and D.M. Heinekey, J. Am. Chem. Soc., 112 (1990) 5166.
D.M. Heinekey and D.M. Oldham, Jr., Chem. Rev., 93 (1993) 913.
J. Gouchen and R.H. Morris, J. Am. Chem. Soc., 113 (1991) 875.
[70] F. van Gastel, J.F. Corrigan, S. Doherty and N.J. Taylor, Inorg. Chem., 31 (1992) 4492.
[71] B.K. Teo, X. Shi and H. Zhang, J. Am. Chem. Soc., 114 (1992) 2743.
[72] G. Schmid, R. Pfeil, R. Boese, F. Bandermann, S. Meyer, G.H.M. Callis and J.W.A. van der Velden, Chem. Ber., 114 (1981) 3634.
G. Schmid, Struct. Bonding, 62 (1985) 51.
G. Schmid, N. Klein, L. Korste, U. Kreibig and D. Schönaure, Polyhedron, 7 (1988) 2321.
[73] M.N. Vargaftik, V.P. Zagorodnikov, I.P. Stolarov, I.I. Moiseev, D.I. Kochubey, V.A. Likholobov, A.L. Chuvilin and K.I. Zamaraev, J. Mol. Catal., 53 (1989) 315.
[74] M. Moskovits, in D.R. Salahub and N. Russo (eds.), Metal–Ligand Interactions: From Atoms, to Clusters, to Surfaces, Kluwer, Dordrecht, 1992, p. 1.
[75] C.J. McNeal, R.E.P. Winpenny, J.M. Hughes, R.D. Macfarlane, L.H. Pignolet, L.T.J. Nelson, T.G. Gardner, L.H. Irgens, G. Vigh and J.P. Fackler, Jr., Inorg. Chem., 32 (1993) 5582.
H. Feld, A. Leute, D. Rading, A. Benninghoven and G. Schmidt, J. Am. Chem. Soc., 112 (1990) 8166.
H. Feld, A. Leute, D. Rading, A. Benninghoven and G. Schmid, Z. Phys. D, 17 (1990) 73.